

A new avialan theropod from an emerging Jurassic terrestrial fauna

<https://doi.org/10.1038/s41586-023-06513-7>

Received: 4 April 2023

Accepted: 2 August 2023

Published online: 6 September 2023

 Check for updates

Liming Xu^{1,5}, Min Wang^{2,5✉}, Runsheng Chen¹, Liping Dong², Min Lin¹, Xing Xu^{2,3,4}, Jianrong Tang¹, Hailu You², Guowu Zhou¹, Linchang Wang¹, Wenxing He¹, Yujuan Li¹, Chi Zhang² & Zhonghe Zhou²

Birds are descended from non-avialan theropod dinosaurs of the Late Jurassic period, but the earliest phase of this evolutionary process remains unclear owing to the exceedingly sparse and spatio-temporally restricted fossil record^{1–5}. Information about the early-diverging species along the avialan line is crucial to understand the evolution of the characteristic bird bauplan, and to reconcile phylogenetic controversies over the origin of birds^{3,4}. Here we describe one of the stratigraphically youngest and geographically southernmost Jurassic avialans, *Fujianvenator prodigiosus* gen. et sp. nov., from the Tithonian age of China. This specimen exhibits an unusual set of morphological features that are shared with other stem avialans, troodontids and dromaeosaurids, showing the effects of evolutionary mosaicism in deep avialan phylogeny. *F. prodigiosus* is distinct from all other Mesozoic avialan and non-avialan theropods in having a particularly elongated hindlimb, suggestive of a terrestrial or wading lifestyle—in contrast with other early avialans, which exhibit morphological adaptations to arboreal or aerial environments. During our fieldwork in Zhenghe where *F. prodigiosus* was found, we discovered a diverse assemblage of vertebrates dominated by aquatic and semi-aquatic species, including teleosts, testudines and choristoderes. Using in situ radioisotopic dating and stratigraphic surveys, we were able to date the fossil-containing horizons in this locality—which we name the Zhenghe Fauna—to 148–150 million years ago. The diversity of the Zhenghe Fauna and its precise chronological framework will provide key insights into terrestrial ecosystems of the Late Jurassic.

Our understanding of the earliest evolutionary history of the Avialae, the most inclusive clade that contains all modern birds but not *Deinonychus* or *Troodon*⁶, has been hampered by the limited diversity of fossils from the Jurassic period, when avialans diverged from the main line of theropods^{1,4,7}. Specifically, few avialans have been reported from localities other than the Middle–Late Jurassic Yanliao Biota in north-east China (166–159 million years ago (Ma)) and the slightly younger Solnhofen Limestones in Germany (the latter site lacks radioisotopic dates)^{2,8–10}, leaving a gap of approximately 30 million years until the oldest known record of Cretaceous avialans—the *Protopteryx*-bearing Huajiyang Formation³. The earliest diverging avialans are key to deciphering the evolutionary origin of the characteristic avialan morphologies that contributed to their first global-scale diversification in the Cretaceous^{3,4}, and, more importantly, to revealing the increasingly complex evolutionary history of stem avialans^{2,7,11}. Here we describe a newly identified avialan, *Fujianvenator prodigiosus* gen. et sp. nov., from the Upper Jurassic of southeastern China. Our comparative analyses show that *Fujianvenator* is distinct from all other Mesozoic avialan and non-avialan theropods in the architecture of its hindlimbs, but

not that of the forelimbs. The unusually elongated lower leg and other morphologies of *Fujianvenator*, combined with geological and palaeontological data from the Zhenghe locality, suggest that it lived in a swamp-like environment—a previously unknown ecological niche for early avialans. Our fieldwork uncovered more than 100 well-preserved vertebrate fossils from the Zhenghe locality, constituting a promising new Late Jurassic terrestrial lagerstätte, which we name the Zhenghe Fauna.

Systematic palaeontology

Theropod Marsh, 1881
Maniraptora Gauthier, 1986
Avialae Gauthier, 1986
Fujianvenator prodigiosus gen. et sp. nov.

Etymology. ‘Fujian’ (Mandarin), referring to Fujian Province, where the holotype was discovered; ‘venator’, hunter (Latin); ‘prodigiosus’,

¹Fujian Institute of Geological Survey, Fuzhou, China. ²Key Laboratory of Vertebrate Evolution and Human Origins, Institute of Vertebrate Paleontology and Paleoanthropology, Chinese Academy of Sciences, Beijing, China. ³Centre for Vertebrate Evolutionary Biology, Yunnan University, Kunming, China. ⁴Paleontological Museum of Liaoning, Shenyang Normal University, Shenyang, China. ⁵These authors contributed equally: Liming Xu, Min Wang. ✉e-mail: wangmin@ivpp.ac.cn

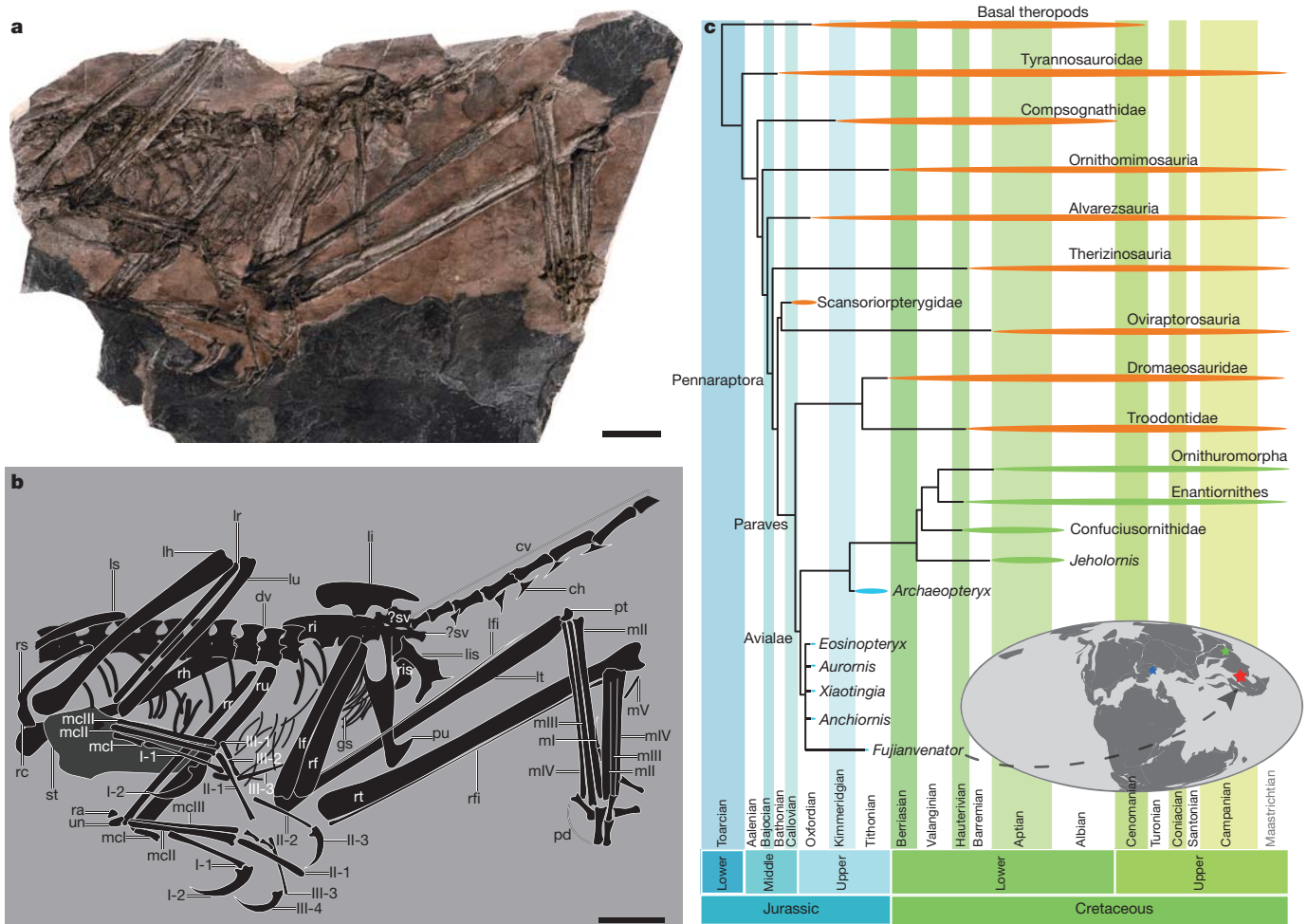


Fig. 1 | Morphology, phylogenetic and palaeogeographical position of *F. prodigiosus*, IVPP V31985. a, b, Photograph (a) and line drawing (b) of the holotype of *F. prodigiosus* (composite drawing based on both the slab and the counter slab). **c**, Time-scaled phylogenetic tree showing the position of *F. prodigiosus* (red star), with a palaeomap of the Late Jurassic (150 Ma) showing the distribution of the known Jurassic avialan fossils. The green and blue stars denote the Yanliao Biota and the Solnhofen Limestones, respectively. See Extended Data Figs. 4 and 5 for complete results of phylogenetic analyses. Abbreviations in **b** are as follows: ch, chevron; cv, caudal vertebra; dv, dorsal

vertebra; gs, gastralia; lf, left femur; lfi, left fibula; lh, left humerus; li, left ilium; lis, left ischium; lr, left radius; ls, left scapula; lt, left tibia; lu, left ulna; ml to mV, metatarsal I to V; mcl to III, metacarpal I to III; pd, pedal digit; pt, proximal tarsal; pu, pubis; rh, right humerus; ra, radiale; rc, right coracoid; rf, right femur; rfi, right fibula; ri, right ilium; ris, right ischium; rr, right radius; rs, right scapula; rt, right tibia; ru, right ulna; st, sternum; un, ulnare; ?sv, possible sacral vertebra; I-1 to I-2, manual phalanx I-1 and I-2; II-1 to II-3, manual phalanx II-1 to II-3; III-1 to III-4, manual phalanx III-1 to III-4. Scale bars, 20 mm.

bizarre (Latin), referring to the odd hindlimb morphology preserved in this species.

Holotype. Institute of Vertebrate Paleontology and Paleoanthropology (IVPP) V31985, an articulated and partially complete skeleton preserved on a slab and counter slab (Fig. 1, Extended Data Fig. 1 and Supplementary Table 1).

Locality and horizon. Near Yangyuan Village, Zhenghe County, Nanping City, Fujian Province; Upper Jurassic, Nanyuan Formation (Tithonian stage; 149.9–150.2 Ma; see Methods).

Diagnosis. *Fujianvenator* differs from all other paravians in the following combination of features (* indicates probable autapomorphy): chevrons located posterior to the fourth caudal vertebra twice longer anteroposteriorly than dorsoventrally; scapula less than half the length of the humerus; sternum ossified; humerus longer than femur; metacarpals I and II that have asymmetric ginglymoid distal articulations with enlarged medial condyles* (the three manual digits of maniraptorans are here denoted as I, II and III, following a previous study¹²); ungual of manual digit I much larger than that of other digits; manual phalanx II-1 longer than II-2; pubic apron mediolaterally broad and imperforated; short ischium that has a distally located obturator

process and a posterior process distally located*; elongated tibia twice as long as the femur*; and metatarsal II mediolaterally wider than other metatarsals.

Description

IVPP V31985 is an avialan around the size of a koklass pheasant, with a body mass of approximately 641 g (estimated using an empirical equation based on the diameter of the femur shaft¹³). The specimen is not skeletally mature, given the unfused metacarpals and tibiotarsus. On the basis of the closed neurocentral sutures of the dorsal vertebrae, the fused astragalus and calcaneum and the ossified sternum, we interpret IVPP V31985 as a subadult.

The trunk is almost complete and consists of 10–12 articulated vertebrae (Fig. 1a,b and Extended Data Fig. 1). As in *Archaeopteryx* and *Anchiornis*^{9,14}, the rectangular neural spines of the middle and posterior dorsal vertebrae are posteriorly located and slightly expand posteriorly along their dorsal margins. The incomplete tail preserves only eight anterior vertebrae with recognizable features (Fig. 2a,b). Considering the articulated vertebral column, the proximity of the ilium and

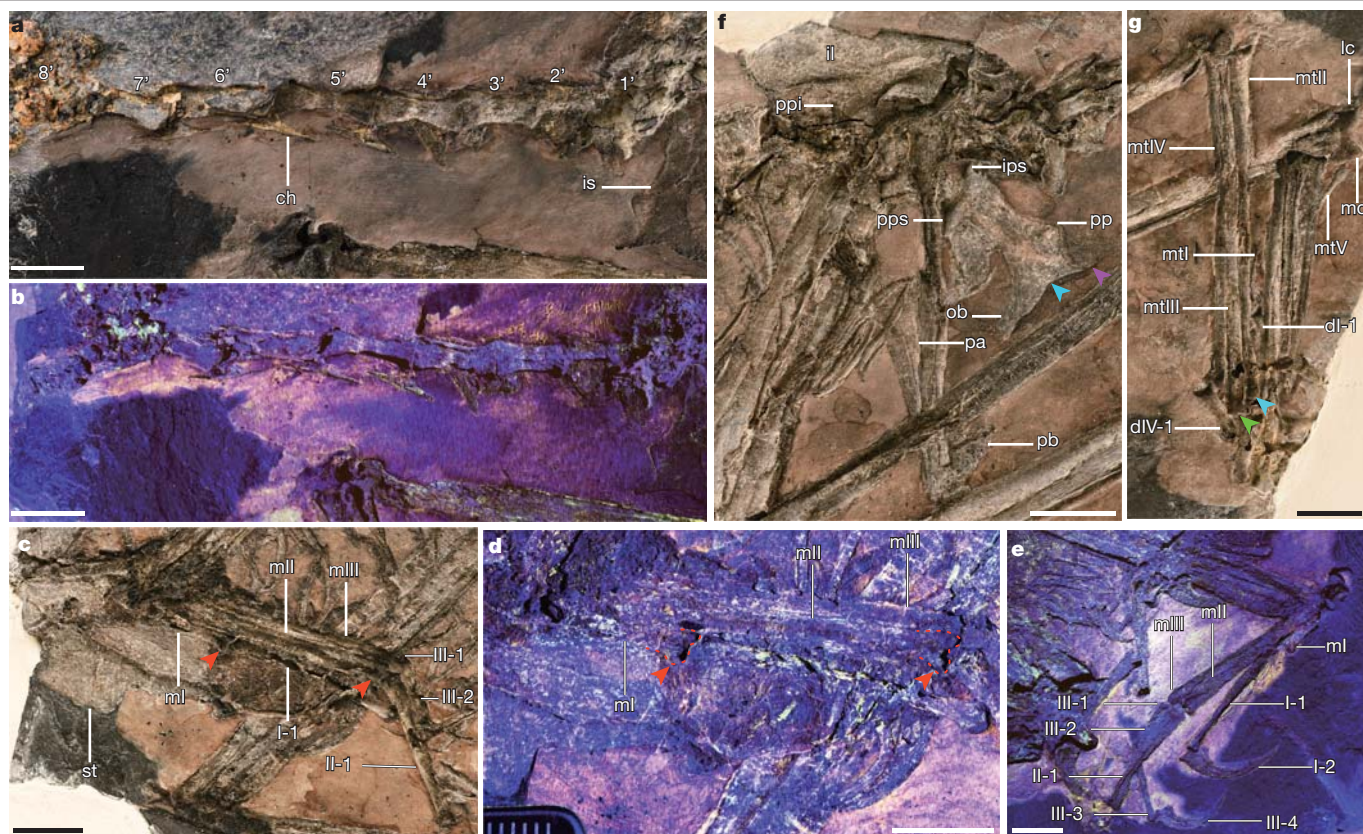


Fig. 2 | Anatomy of *F. prodigiosus*, IVPP V31985. a, b, Photograph of caudal vertebrae under normal light (a) and under laser light (b). The numbers 1' to 8' denote the recognized first to eighth caudal vertebrae. **c**, Left hand. **d**, Magnified view of left metacarpals I and II under laser light. The red arrowheads in **c, d** show the asymmetric ginglymoid distal articulations of metacarpals I and II. **e**, Right hand under laser light. **f**, Pelvis. Purple arrowhead denotes the elongated tapering posterodistal end; blue arrowhead shows the constriction at the base of the obturator process. **g**, Metatarsals. Green and

blue arrowheads denote the ginglymoid metatarsal III and non-ginglymoid metatarsal II, respectively. Abbreviations as follows: ch, chevron; dI-1, pedal phalanx I-1; dIV-1, pedal phalanx IV-1; ips, iliac peduncle of ischium; is, ischium; lc, lateral condyle; mc, medial condyle; ml to mIII, metacarpal I to III; mtl to mtV, metatarsal I to V; ob, obturator process; pa, pubic apron; pb, pubic boot; ppi, pubic peduncle of ilium; pp, posterior distal process; pps, pubic peduncle of ischium; st, sternum; I-1 and I-2, manual phalanx I-1 and I-2; II-1, manual phalanx II-1; III-1 to III-4, manual phalanx III-1 to III-4. Scale bars, 10 mm.

caudal vertebrae and the position of two possible caudalmost sacral vertebrae, one or two additional vertebrae might have been present anterior to those eight centra. The length of these vertebrae increases more rapidly than in *Archaeopteryx*, but is comparable to the case in *Jeholornis*¹⁵, with the fifth vertebra being twice as long as the first one. The chevrons located posterior to the fourth caudal vertebra are twice as long anteroposteriorly than dorsoventrally, and the anterior extension is longer than the posterior one. By contrast, in *Archaeopteryx* and *Anchiornis*^{9,14} the chevrons in equivalent locations are rectangular and dorsoventrally deep. The ribs are curved and associated with the dorsal vertebrae. The gastralia are more delicate than the ribs and taper at both ends.

The scapula measures approximately 40% of the length of the humerus, and is substantially shorter than in other theropods, including *Anchiornis* and *Xiaotingia*, in which the ratio is greater than 60% (ref. 16). A large, plate-like element is preserved in the chest and close to the right coracoid (Figs. 1a and 2c). We tentatively interpret it as the sternum, given its size and position. If this is the case, *Fujianvenator* represents the second oldest record so far of an ossified sternum, and is only stratigraphically younger than the scansoriopterygid *Epidexipteryx* among maniraptoran theropods^{2,17}.

The humerus is considerably longer than the femur (ratio of around 1.38)—reminiscent of, but to a greater extent than, the condition in Cretaceous avialans—whereas the opposite is true in other non-avian theropods, except the scansoriopterygids^{18,19} (Supplementary Table 2). As in other Jurassic paravians^{7,9,20}, the humerus has a small deltopectoral

crest and a distal margin that is perpendicular to the longitudinal axis of the shaft. Similar to most non-avian theropods^{19,21}, the ulna is shorter than the humerus. As in *Anchiornis* and *Eosinopteryx*^{14,22}, but unlike other paravians such as *Archaeopteryx* and many deinonychosaur^{2,9,23}, the ulna is straight. The olecranon process is poorly developed. The radius measures approximately 80% of the width of the ulna. The metacarpals are unfused with one another or with the proximal carpals (Fig. 2c–e). Metacarpal I is approximately one-quarter of the length of metacarpal II, proportionally shorter than in *Anchiornis*¹⁴, troodontids^{24,25} and dromaeosaurids^{26,27}, but comparable to that of *Archaeopteryx* and more crownward taxa^{28,29}. Metacarpals I and II terminate in asymmetrical ginglymoid articulations in which the hypertrophied medial condyle projects medially well beyond the medial margin of the shaft (Fig. 2d and Extended Data Fig. 2a, b), a feature that is unknown in other theropods^{30,31}. As in most paravians, but not in *Xiaotingia* or enantiornithines^{2,7,32}, metacarpal II extends further distally than metacarpal III. Metacarpal III is straight and appressed to metacarpal II, rather than being bowed laterally as in many paravians^{14,33}. The slender metacarpal III is less than half the width of metacarpal II, similar to *Anchiornis* and *Alcmonavis*³¹. By contrast, metacarpal III is the most robust metacarpal in *Xiaotingia*⁷. The manual phalangeal formula is 2-3-4, and the phalangeal portion is much longer than the metacarpus, as in *Xiaotingia*, *Archaeopteryx* and some oviraptorosaurs⁷. The unguals have prominent flexor processes proximally. Similar to *Archaeopteryx*²⁹, the longest non-ungual phalanx is I-1, rather than being II-2 as in *Xiaotingia* and *Anchiornis*^{7,14}. Digit I (excluding the ungual) is

as long as metacarpal II, representing an intermediate stage from the ancestral theropod condition to the shortened form in later-diverging avialans^{2,27,34,35}. The ungual of digit I is much larger than that of other digits (Fig. 2e), a feature absent in most non-avian theropods, *Anchiornis*¹⁴ and *Archaeopteryx*^{2,9} but present in many Cretaceous avialans^{16,36}. In contrast to what is seen in early-diverging theropods and Jurassic paravians^{2,34,37}, phalanx II-1 is longer than II-2, a derived condition of avialans³⁶. As in most non-avian theropods, phalanx II-1 is as gracile as other non-ungual manual phalanges^{23,27,34}. By contrast, it is the most robust phalanx in *Anchiornis*, *Alcmonavis* and more crownward taxa^{3,31}. As in *Anchiornis*¹⁴, phalanges III-1 and III-2 are nearly equal in length, in stark contrast to the large difference between them that is present in other paravians, such as *Archaeopteryx* and *Xiaotingia*⁷.

The ilium is convex anteriorly, which contrasts with both the concave form, as in *Anchiornis* and some dromaeosaurids^{2,14}, and the straight condition, as in some troodontids³⁸ (Fig. 2f and Extended Data Figs. 2c and 3). The pubes meet extensively and form a mediolaterally broad apron distally (Fig. 2f), a feature unique to troodontids among theropods³⁹. A slit-like opening in the middle of the apron, which is widely distributed among dromaeosaurids^{2,40,41}, is absent. The pubic apron extends over half the length of the shaft, and is proportionally longer than in *Anchiornis* and early avialans^{2,20}. The pubic boot has a posterior triangular expansion, similar to that of *Anchiornis* and *Archaeopteryx*⁷. The strap-like ischium measures one-third of the length of the pubis—proportionally shorter than in many paravians⁷. The obturator process is distally located and constricted at its base, a feature that is only observed in *Archaeopteryx* and *Anchiornis* among theropods⁷ (Extended Data Fig. 3). Specifically, this process is more proximally located and lacks the constriction in other paravians, including *Aurornis* and deinonychosaurs^{2,42}. Unlike other Jurassic paravians, except *Archaeopteryx*^{7,22,39}, the ischium has a posterior process that is distally located (Fig. 2f and Extended Data Fig. 2c). A second and proximally located posterior process that is present in *Archaeopteryx* and many troodontids^{7,43}, is absent; this process is more prominent in later-diverging avialans^{3,32}. The ischium terminates with a tapered posterior end that projects posteriorly prominently, as in *Anchiornis*, rather than being ventrally directed as in *Archaeopteryx*⁹; by contrast, that end is blunt in deinonychosaurs^{26,43} (Extended Data Fig. 3).

The robust femur is straight, and the hyperelongated tibia is twice as long as the femur, markedly exceeding the ratio in all other known Mesozoic theropods¹⁸ (Supplementary Table 3). The astragalus and calcaneum are fused with each other, but not to the tibia. The medial condyle is mediolaterally wider than the lateral condyle (Fig. 2g and Extended Data Fig. 2d), a plesiomorphic condition in theropods³⁶. The splint-like fibula extends distally and nearly contacts the lateral condyle. The gracile metatarsus is slightly longer than the femur, but the opposite is true in most other theropods^{18,44}. Metatarsal I articulates with the medial side of metatarsal II at its mid-length (Fig. 2g), whereas it is more distally located in other paravians^{16,45}. As in stem avialans such as *Anchiornis*^{14,46}, metatarsal III is not pinched proximally, contrasting with the sub- or arctometatarsal condition that is observed in troodontids and many non-avian theropods^{47,48}. Metatarsals II and IV terminate distally level with the proximal margin of metatarsal III trochlea. As in some dromaeosaurids⁴⁹, *Archaeopteryx* and some enantiornithines^{9,46}—but unlike other paravians including *Anchiornis*^{14,42}—metatarsal II is mediolaterally wider than the other metatarsals (Fig. 2g and Extended Data Fig. 2d). By contrast, troodontids characteristically have a metatarsal IV that is longer and stouter than metatarsal II^{47,48}. As in *Anchiornis*, *Archaeopteryx* and troodontids^{9,47,48}, metatarsal II lacks the ginglymoid distal articulation that is present in dromaeosaurids⁵⁰ (Fig. 2g). Unlike in *Archaeopteryx* and some troodontids (for example, *Sinornithosaurus* and *Jianianhua*)^{2,9,39}, metatarsal III is ginglymoid, a plesiomorphic condition for paravians^{47,50}. The vestigial metatarsal V is less than one-seventh of the length of metatarsal III—proportionally

shorter than in *Anchiornis* and some dromaeosaurids^{14,41}. The proximal pedal phalanges are spool-shaped and have well-developed ginglymoid distal facets.

Morphometric analyses

To compare the body shape of IVPP V31985 with that of other Mesozoic avialan and non-avian theropods, phylogenetic principal component analysis (pPCA) was performed to investigate changes in limb proportion across theropod evolution (Fig. 3). pPCA of all limbs shows that PC1 correlates nearly equally with all limb segments, indicating that it mainly describes overall size changes (Supplementary Table 4). PC2 shows opposite signs of eigenvector coefficients with forelimb and hindlimb, respectively, and thus it describes the elongation of the forelimb relative to the hindlimb. Avialans are well separated from basal non-avian theropods along this axis (Extended Data Fig. 4a). The eigenvector coefficients of PC3 show that it reflects the elongation of metacarpal III relative to the humerus and ulna. Phylomorphospace of the first three principal components (PCs) (accounting for around 92% of the variance) shows that *Fujianvenator*, *Archaeopteryx* and *Anchiornis* are located close to one another, and that together they occupy an intermediate position between the morphospace of the non-avian theropods and that of other avialans (Fig. 3a and Extended Data Fig. 4a,b).

pPCA of the forelimb shows that PC1 corresponds to the overall size of the forelimb, and thus large-bodied non-avian theropods are widely separated from avialans along this axis (Supplementary Table 5). PC2 reflects the relative elongation of metacarpal II, and PC3 describes the elongation of the humerus relative to the ulna. The phylomorphospace of the forelimb is largely comparable to that of the six limb segments, and resolves these Jurassic avialans in an intermediate position between the morphospaces of the non-avian theropods and those of other avialans (Fig. 3b and Extended Data Fig. 4c,d). pPCA of the hindlimb shows that PC1 negatively correlates with the femur, tibia and metatarsal III, with subequal loading of eigenvector coefficients (Supplementary Table 5); differences along this axis distinguish most large-bodied non-paravian theropods from avialans (Fig. 3c and Extended Data Fig. 4e,f). PC2 reflects the elongation of the femur relative to metatarsal III. PC3 corresponds to the elongation of the tibia with respect to other segments, with *Fujianvenator* and the flightless ornithomorph *Patagopteryx* exhibiting the lowest scores. Notably, *Fujianvenator* is located far away from all other avialan and non-avian theropods in hindlimb morphospace. Similar results were obtained using conventional PCA without accounting for phylogeny (Supplementary Figs. 1 and 2). Together, our pPCA analyses show that the resemblance between *Fujianvenator* and other avialans in overall bauplan is mainly driven by forelimb changes, despite the unique hindlimb architecture that evolved in *Fujianvenator*.

Discussion

Our phylogenetic analyses consistently recovered *Fujianvenator* within the clade Anchiornithidae, which unites other *Anchiornis*-like taxa⁵¹ and is resolved as the earliest diverging group of the Avialae (Fig. 1b). *Archaeopteryx* was resolved within the Avialae as the sister to other avialans except the anchiornithids. This result is robust to maximum parsimony and Bayesian analyses using tip-dating methods (Extended Data Figs. 5 and 6). Given that it is at present the southernmost record of Jurassic avialans, and is 10 million years younger than the Yanliao taxa (Fig. 1b), *Fujianvenator* contributes a great deal of spatio-temporal information about early avialan diversification close to the end of the Jurassic. *Fujianvenator* is largely comparable with *Archaeopteryx* in having similar manual phalangeal proportions. On the other hand, its pelvis shows features that are used to diagnose *Anchiornis* and troodontids (Extended Data Fig. 3): the short ischium is *Anchiornis*-like, bearing

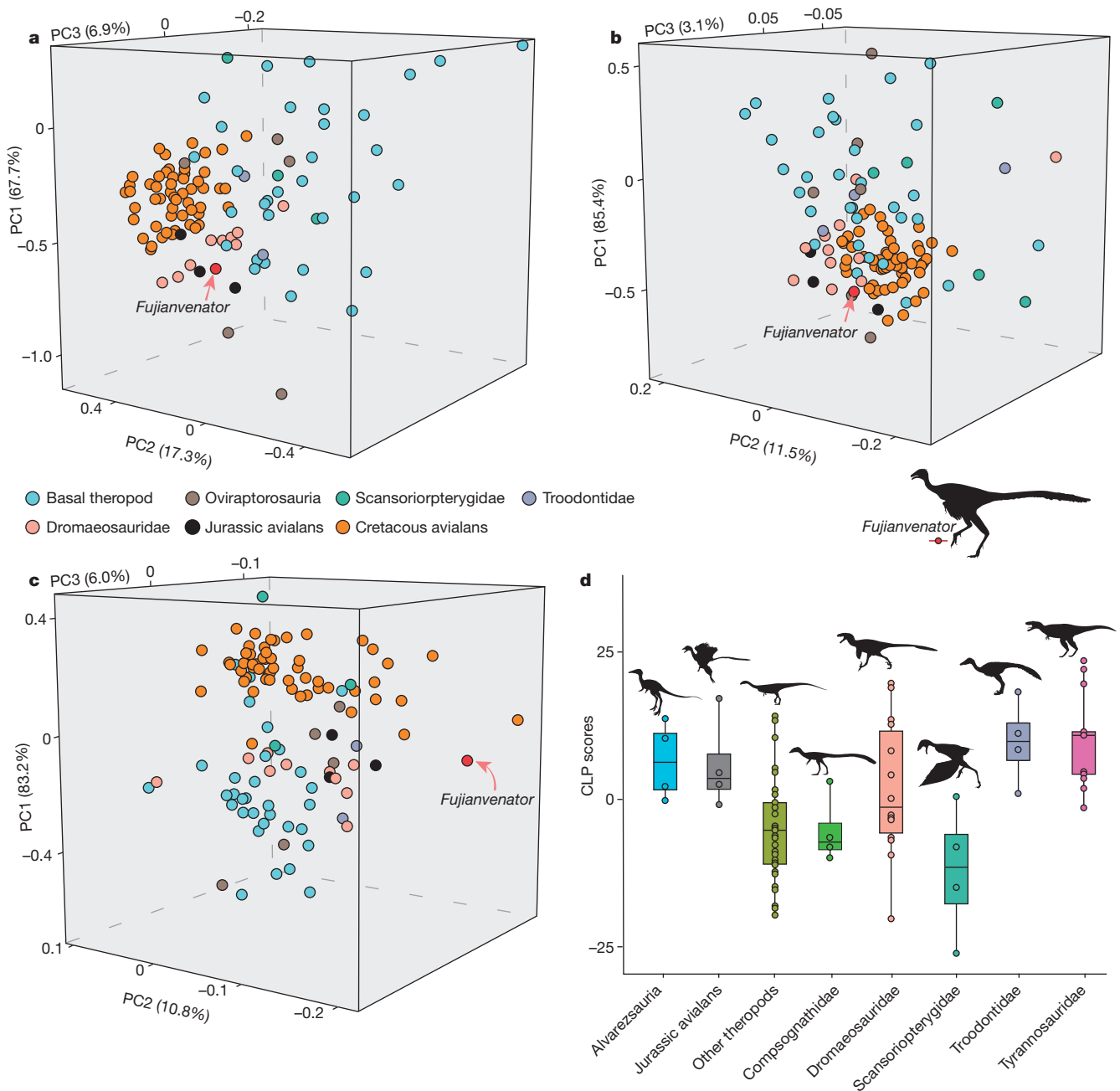


Fig. 3 | Three-dimensional morphometric space of limb bones and cursoriality of Mesozoic theropods. a–c. First three PCs of pPCAs of the lengths of six limb segments (a), forelimb (b) and hindlimb (c). **d.** Box plots showing the cursoriality of selected Mesozoic theropods on the basis of cursorial limb proportion (CLP) scores ($n = 78$ independent taxa compared with *Fujianvenator*). Alvarezsauria: minimum = -0.17 , 1st quartile = 1.62 , centre = 6.29 , 3rd quartile = 11.20 , maximum = 13.70 ; Jurassic avialans: minimum = -0.84 , 1st quartile = 1.71 , centre = 3.56 , 3rd quartile = 7.70 , maximum = 7.70 ; other theropods: minimum = -19.67 , 1st quartile = -10.99 , centre = -5.23 , 3rd quartile = -0.56 , maximum = 14.04 ; Compsognathidae:

minimum = -9.91 , 1st quartile = -8.54 , centre = -7.24 , 3rd quartile = -4.03 , maximum = -4.03 ; Dromaeosauridae: minimum = -20.25 , 1st quartile = -5.70 , centre = -1.33 , 3rd quartile = 11.58 , maximum = 19.72 ; Scansoriopterygidae: minimum = -26.04 , 1st quartile = -17.72 , centre = -11.50 , 3rd quartile = -5.94 , maximum = 0.42 ; Troodontidae: minimum = 1.01 , 1st quartile = 6.61 , centre = 9.83 , 3rd quartile = 12.95 , maximum = 18.24 ; Tyrannosauridae: minimum = -1.46 , 1st quartile = 4.26 , centre = 10.86 , 3rd quartile = 11.47 , maximum = 22.04 . See Extended Data Fig. 6 for binary plots. Silhouettes except *Ambopteryx* (modified from a previous report¹⁹) and *Fujianvenator* are adapted from PhyloPic under the Creative Commons licence CC0.1.0 (list in the Supplementary Information).

a distally located obturator process that is constricted at its base⁷²⁰, whereas the pubes resemble these of troodontids in having a mediolaterally broad, proximodistally elongated imperforated apron³⁹. Notably, the hindlimb of *Fujianvenator* exhibits mixed morphologies in its finer aspects, including non-arcometatarsal feet like those in *Archaeopteryx* and *Anchiornis*⁹¹⁴; a metatarsal II that is mediolaterally broader than metatarsals III and IV, as in *Archaeopteryx*³¹; a non-ginglymoid metatarsal II,

as in troodontids^{47,48}; a metatarsal II trochlea that is wider than that of other metatarsals, as in *Anchiornis* and some dromaeosaurids^{44,49}; and a ginglymoid metatarsal III, as in dromaeosaurids and some troodontids³³ (Fig. 2g and Extended Data Figs. 2d and 3). The unique combination of postcranial features shared with early avialans that is preserved in *Fujianvenator* shows how deeply the avialan phylogeny has been affected by evolutionary mosaicism. That, in turn, partly

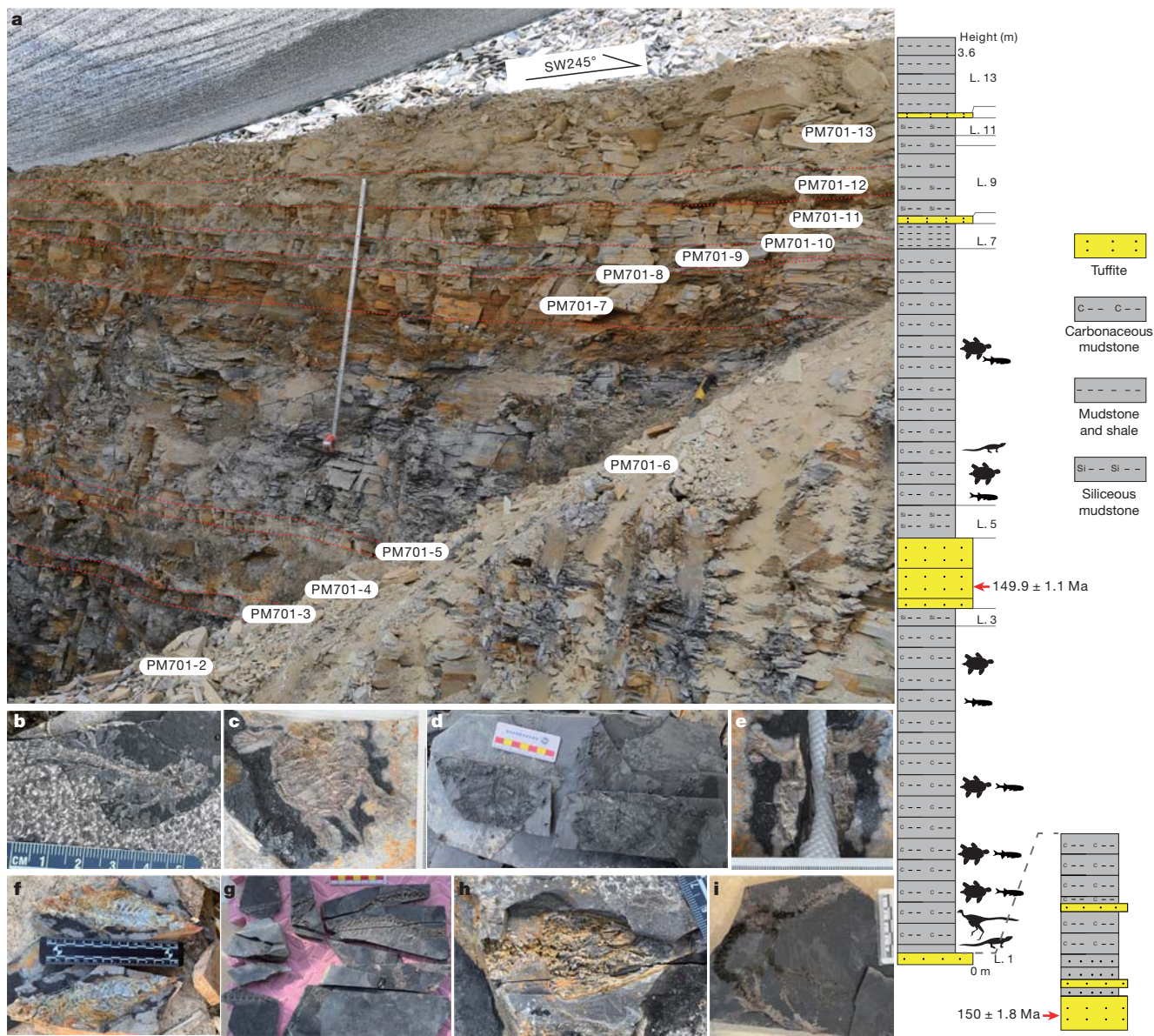


Fig. 4 | Stratigraphic log and vertebrate fossil assemblage discovered from the Late Jurassic Zhenghe Fauna. **a**, Photograph and composite stratigraphic log of the excavation site, showing the fossil-bearing horizons and the localities of radiometrically dated horizons. SW245° denotes the strike direction of the

section; L. denotes layer. **b–i**, Photos of vertebrate fossils that were discovered during the 2022 fieldwork in Zhenghe. **b**, Teleostei indeterminate (indet.) (Actinopterygii: Neopterygii). **c–e**, Testudines indet. (Reptilia: Pantestudines). **f–i**, Allochoristodera indet. (Reptilia: Choristodera).

explains the controversy about the interrelationships among these early-diverging paravians^{1,2,7,52}.

Functional morphological changes along the line to avialans have long been ascribed to selection relating to powered flight; for example, reduction in body size and elongation of the forelimbs^{4,53,54}. However, unlike other Jurassic avialans^{4,20,39}, *Fujianvenator* preserves few skeletal modifications that might have contributed to the refinement of aerial performance. For instance, metacarpal II and its associate digit are gracile, rather than being robust as in *Anchiornis* and more crownward taxa, where they serve as the attachment for primary remiges^{14,31}; and metacarpals I and II are strongly ginglymoid with an enlarged medial condyle (Fig. 2c,d)—indicative of a high degree of flexion (which would aid prey capture, for example)—rather than forming an immobile unit for feather attachment⁵⁵. The gracile and elongated hindlimb, combined with the proximally located hallux (also seen in later-diverging deinonychosaurs with terrestrial habits⁴⁵), instead implies cursorial adaptation⁵⁶. When all the limb segments or only the forelimb are analysed

in pPCA, *Fujianvenator* is located close to other Jurassic avialans in morphospace, and they occupy an intermediate position between the morphospaces of avialan and non-avialan theropods (Fig. 3a,b and Extended Data Fig. 4a–d). However, when only the hindlimb is analysed, *Fujianvenator* is located far away from all other theropods, including other Jurassic avialans (Fig. 3d and Extended Data Fig. 4e,f). These results show that marked changes in body plan occurred along the stem avialan line, largely driven by the forelimb (principal components mainly aligned with forelimb variables; Supplementary Tables 4 and 5) and eventually giving rise to the typical limb proportions of crown birds (for example, an ulna that is longer than the humerus). *Fujianvenator* is an example of an avialan that diverged from this main trajectory and evolved bizarre hindlimb architecture; however, that transformation has been overshadowed by changes in the forelimb.

The unusual hindlimb proportion of *Fujianvenator* still holds true when it is compared with a phylogenetically broad sample of crown birds that encompass diverse ecomorphologies (Extended Data Fig. 7).

The elongation of the lower leg—tibia and metatarsus—is generally considered an index of running speed among modern vertebrates^{56,57}, because of the increased stride length⁵⁸. We used a quantifiable measure of cursoriality⁵⁸ to compare *Fujianvenator* with other major theropod groups. *Fujianvenator* was recovered with a cursorial score that was substantially higher than that of other non-avian theropods, including troodontids and tyrannosaurids, which have long been viewed as good runners^{48,58} (Fig. 3d). These results show that *Fujianvenator* was well adapted for terrestrial locomotion and is likely to have been capable of running at a high speed—consistent with the terrestrial-related skeletal features mentioned above. Elongated lower legs are also present in some crown birds, such as waders (for example, storks and cranes), and *Fujianvenator* is located close to the hindlimb morphospace of those crown taxa, suggesting that a wading ecology is equally possible for this taxon. Unfortunately, the pedal digits, which are pertinent functionally to locomotion strategy and thus could help distinguish cursoriality from wading ecology, are poorly preserved, meaning that the ecology of *Fujianvenator* remains an open question at this point.

The *Fujianvenator*-bearing horizon of the Nanyuan Formation is composed of black carbonaceous mudstone and shale, interstratified with tuffite⁵⁹ (Fig. 4a). The assemblage of vertebrate fossils discovered in this area is dominated by aquatic and semi-aquatic vertebrates, such as teleosts, testudines and choristoderes (Fig. 4 and Extended Data Fig. 8). These geological and palaeontological data lead us to interpret *Fujianvenator* as an agile predator or a wader living in a swamp-like environment (Methods)—different from those Yanliao avialans (for example, *Anchiornis*) that show morphological features for arboreal adaptation⁸. The Nanyuan Formation and contemporaneous deposits distributed in Zhenghe are certainly fossiliferous—more than 100 reptile fossils, most of them well preserved, were discovered in our month of fieldwork (Fig. 4 and Extended Data Fig. 8). The discovery of an avialan, and the abundant choristoderes, the later of which have not been reported from the Yanliao Biota and the Solnhofen Limestones¹⁰, make this locality unique with regard to the early evolution of these lineages. The sheer diversity of fossils, and the distinctive palaeoenvironment, combined with the precise age constraints of the fossil-bearing horizons (148–150 Ma; see Methods), show the great potential of Zhenghe as an emerging Jurassic vertebrate fauna that fills a key temporal and geological gap in our understanding of the ecosystems of northeast Asia in the Late Jurassic.

Online content

Any methods, additional references, Nature Portfolio reporting summaries, source data, extended data, supplementary information, acknowledgements, peer review information; details of author contributions and competing interests; and statements of data and code availability are available at <https://doi.org/10.1038/s41586-023-06513-7>.

- Rauhut, O. W. M. & Foth, C. in *The Evolution of Feathers: From Their Origin to the Present* (eds Foth, C. & Rauhut, O. W. M.) 27–45 (Springer, 2020).
- Turner, A. H., Makovicky, P. J. & Norell, M. A. A review of dromaeosaurid systematics and paravian phylogeny. *Bull. Am. Mus. Nat. Hist.* **371**, 1–206 (2012).
- Wang, M. & Zhou, Z. in *The Biology of the Avian Respiratory System* (ed. Maina, N. J.) 1–26 (Springer, 2017).
- Xu, X. et al. An integrative approach to understanding bird origins. *Science* **346**, 1253293 (2014).
- Brusatte, S. L., O'Connor, J. K. & Jarvis, E. D. The origin and diversification of birds. *Curr. Biol.* **25**, R888–R898 (2015).
- Gauthier, J. Saurischian monophyly and the origin of birds. *Mem. Calif. Acad. Sci.* **8**, 1–55 (1986).
- Xu, X., You, H., Du, K. & Han, F. An *Archaeopteryx*-like theropod from China and the origin of Avialae. *Nature* **475**, 465–470 (2011).
- Xu, X., Zhou, Z., Sullivan, C., Wang, Y. & Ren, D. An updated review of the Middle-Late Jurassic Yanliao Biota: chronology, taphonomy, paleontology and paleoecology. *Acta Geol. Sin.* **90**, 2229–2243 (2016).
- Rauhut, O. W., Foth, C. & Tischlinger, H. The oldest *Archaeopteryx* (Theropoda: Avialae): a new specimen from the Kimmeridgian/Tithonian boundary of Schamhaupten, Bavaria. *PeerJ* **6**, e4191 (2018).
- Zhou, Z. & Wang, Y. Vertebrate diversity of the Jehol Biota as compared with other lagerstätten. *Sci. China Earth Sci.* **53**, 1894–1907 (2010).
- Pol, D. & Goloboff, P. A. The impact of unstable taxa in coelurosaurian phylogeny and resampling support measures for parsimony analyses. *Bull. Am. Mus. Nat. Hist.* **440**, 97–115 (2020).
- Bever, G. S., Gauthier, J. A. & Wagner, G. P. Finding the frame shift: digit loss, developmental variability, and the origin of the avian hand. *Evo. Dev.* **13**, 269–279 (2011).
- Benson, R. B. J., Hunt, G., Carrano, M. T. & Campione, N. Cope's rule and the adaptive landscape of dinosaur body size evolution. *Palaeontology* **61**, 13–48 (2018).
- Pei, R., Li, Q., Meng, Q., Norell, M. A. & Gao, K. New specimens of *Anchiornis huxleyi* (Theropoda: Paraves) from the Late Jurassic of northeastern China. *Bull. Am. Mus. Nat. Hist.* **411**, 1–67 (2017).
- Zhou, Z. & Zhang, F. *Feholornis* compared to *Archaeopteryx*, with a new understanding of the earliest avian evolution. *Naturwissenschaften* **90**, 220–225 (2003).
- Li, Z., Wang, M., Stidham, T. A. & Zhou, Z. Decoupling the skull and skeleton in a Cretaceous bird with unique appendicular morphologies. *Nat. Ecol. Evol.* **7**, 20–31 (2023).
- Zheng, X. et al. On the absence of sternal elements in *Anchiornis* (Paraves) and *Sapeornis* (Aves) and the complex early evolution of the avian sternum. *Proc. Natl Acad. Sci. USA* **111**, 13900–13905 (2014).
- Benson, R. B. J. & Choiniere, J. N. Rates of dinosaur limb evolution provide evidence for exceptional radiation in Mesozoic birds. *Proc. R. Soc. B* **280**, 20131780 (2013).
- Wang, M., O'Connor, J. K., Xu, X. & Zhou, Z. A new Jurassic scansoriopterygid and the loss of membranous wings in theropod dinosaurs. *Nature* **569**, 256–259 (2019).
- Hu, D., Hou, L., Zhang, L. & Xu, X. A pre-*Archaeopteryx* troodontid theropod from China with long feathers on the metatarsus. *Nature* **461**, 640–643 (2009).
- Middleton, K. M. & Gatesy, S. M. Theropod forelimb design and evolution. *Zool. J. Linn. Soc.* **128**, 149–187 (2000).
- Godefroit, P. et al. Reduced plumage and flight ability of a new Jurassic paravian theropod from China. *Nat. Commun.* **4**, 1394 (2013).
- Ostrom, J. H. Osteology of *Deinonychus antirrhopus*, an unusual theropod from the Lower Cretaceous of Montana. *Bull. Peabody Mus. Nat. Hist.* **30**, 1–165 (1969).
- Hu, D. et al. A bony-crested Jurassic dinosaur with evidence of iridescent plumage highlights complexity in early paravian evolution. *Nat. Commun.* **9**, 217 (2018).
- Russell, D. A. & Dong, Z. A nearly complete skeleton of a new troodontid dinosaur from the Early Cretaceous of the Ordos Basin, Inner Mongolia, People's Republic of China. *Can. J. Earth Sci.* **30**, 2163–2173 (1993).
- Xu, X., Wang, X. & Wu, X. A dromaeosaurid dinosaur with a filamentous integument from the Yixian Formation of China. *Nature* **401**, 262–266 (1999).
- Nebreda, S. M. et al. Disparity and macroevolutionary transformation of the maniraptoran manus. *Bull. Am. Mus. Nat. Hist.* **440**, 183–203 (2020).
- Wang, M., Wang, X., Wang, Y. & Zhou, Z. A new basal bird from China with implications for morphological diversity in early birds. *Sci. Rep.* **6**, 19700 (2016).
- Mayr, G., Pohl, B., Hartman, S. & Peters, D. S. The tenth skeletal specimen of *Archaeopteryx*. *Zool. J. Linn. Soc.* **149**, 97–116 (2007).
- Xu, X., Han, F. & Zhao, Q. Homologies and homeotic transformation of the theropod 'semilunate' carpal. *Sci. Rep.* **4**, 6042 (2014).
- Rauhut, O. W. M., Tischlinger, H. & Foth, C. A non-archaeopterygid avialan theropod from the Late Jurassic of southern Germany. *eLife* **8**, e43789 (2019).
- O'Connor, J. K. A *Systematic Review of Enantiornithes (Aves: Ornithothoraces)*. PhD thesis, Univ. Southern California (2009).
- Norell, M. A. & Makovicky, P. J. Important features of the dromaeosaurid skeleton II: information from newly collected specimens of *Velociraptor mongoliensis*. *Am. Mus. Novit.* **3282**, 1–45 (1999).
- Zhang, F., Zhou, Z., Xu, X. & Wang, X. A juvenile coelurosaurian theropod from China indicates arboreal habits. *Naturwissenschaften* **89**, 394–398 (2002).
- Xu, X. et al. A Jurassic ceratosaur from China helps clarify avian digital homologies. *Nature* **459**, 940–944 (2009).
- Chiappe, L. M., Ji, S. A., Ji, Q. & Norell, M. A. Anatomy and systematics of the Confuciusornithidae (Theropoda: Aves) from the Late Mesozoic of northeastern China. *Bull. Am. Mus. Nat. Hist.* **242**, 1–89 (1999).
- Zheng, X., Xu, X., You, H., Zhao, Q. & Dong, Z. A short-armed dromaeosaurid from the Jehol Group of China with implications for early dromaeosaurid evolution. *Proc. R. Soc. B* **277**, 211–217 (2010).
- Rhodes, M. M., Henderson, D. M. & Currie, P. J. Maniraptoran pelvic musculature highlights evolutionary patterns in theropod locomotion on the line to birds. *PeerJ* **9**, e10855 (2021).
- Xu, X. et al. Mosaic evolution in an asymmetrically feathered troodontid dinosaur with transitional features. *Nat. Commun.* **8**, 14972 (2017).
- Longrich, N. R. & Currie, P. J. A microraptorine (Dinosauria—Dromaeosauridae) from the Late Cretaceous of North America. *Proc. Natl Acad. Sci. USA* **106**, 5002–5007 (2009).
- Norell, M. A. & Makovicky, P. J. Important features of the dromaeosaur skeleton: information from a new specimen. *Am. Mus. Novit.* **3215**, 1–51 (1997).
- Godefroit, P. et al. A Jurassic avialan dinosaur from China resolves the early phylogenetic history of birds. *Nature* **498**, 359–362 (2013).
- Xu, X., Norell, M. A., Wang, X., Makovicky, P. J. & Wu, X. A basal troodontid from the Early Cretaceous of China. *Nature* **415**, 780–784 (2002).
- Hedrick, B. P., Manning, P. L., Lynch, E. R., Cordero, S. A. & Dodson, P. The geometry of taking flight: limb morphometrics in Mesozoic theropods. *J. Morphol.* **276**, 152–166 (2014).
- Hattori, S. Evolution of the hallux in non-avian theropod dinosaurs. *J. Vertebr. Paleontol.* **36**, e1116995 (2016).
- Wang, M. et al. An Early Cretaceous enantiornithine bird with a pintail. *Curr. Biol.* **31**, 4845–4852 (2021).
- Xu, X. & Wang, X. L. Troodontid-like pes in the dromaeosaurid *Sinornithosaurus*. *Paleontol. Soc. Korea Spec. Publ.* **4**, 179–188 (2000).
- Makovicky, P. J. & Norell, M. A. in *The Dinosauria* (eds Weishampel, D., Dodson, P. & Osmólska, H.) 184–195 (Univ. California Press, 2004).

49. Xu, X. & Wang, X. A new dromaeosaur (Dinosauria: Theropoda) from the Early Cretaceous Yixian Formation of western Liaoning. *Vertebr. Palasiat.* **42**, 111–119 (2004).
50. Norell, M. A. & Makovicky, P. J. in *The Dinosauria* (eds Weishampel, D., Dodson, P. & Osmólska, H.) 196–209 (Univ. California Press, 2004).
51. Foth, C. & Rauhut, O. W. M. Re-evaluation of the Haarlem *Archaeopteryx* and the radiation of maniraptoran theropod dinosaurs. *BMC Evol. Biol.* **17**, 236 (2017).
52. O'Connor, J. K. & Sullivan, C. Reinterpretation of the Early Cretaceous maniraptoran (Dinosauria: Theropoda) *Zhongornis haoae* as a scansoriopterygid-like non-avian, and morphological resemblances between scansoriopterygids and basal oviraptorosaurs. *Vertebr. Palasiat.* **52**, 3–30 (2014).
53. Lee, M. S. Y., Cau, A., Naish, D. & Dyke, G. J. Sustained miniaturization and anatomical innovation in the dinosaurian ancestors of birds. *Science* **345**, 562–566 (2014).
54. Dececchi, T. A. & Larsson, H. C. E. Body and limb size dissociation at the origin of birds: Uncoupling allometric constraints across a macroevolutionary transition. *Evolution* **67**, 2741–2752 (2013).
55. Lovette, I. J. & Fitzpatrick, J. W. *Handbook of Bird Biology* 3rd edn (John Wiley & Sons, 2016).
56. Gatesy, S. M. & Middleton, K. M. Bipedalism, flight, and the evolution of theropod locomotor diversity. *J. Vertebr. Paleontol.* **17**, 308–329 (1997).
57. Christiansen, P. Locomotion in terrestrial mammals: the influence of body mass, limb length and bone proportions on speed. *Zool. J. Linn. Soc.* **136**, 685–714 (2002).
58. Persons, W. S. & Currie, P. J. An approach to scoring cursorial limb proportions in carnivorous dinosaurs and an attempt to account for allometry. *Sci. Rep.* **6**, 19828 (2016).
59. Bureau of Geology and Mineral Resources of Fujian Province. *Lithostratigraphy of Fujian Province* (China Univ. Geosciences Press, 2016).

Publisher's note Springer Nature remains neutral with regard to jurisdictional claims in published maps and institutional affiliations.

Springer Nature or its licensor (e.g. a society or other partner) holds exclusive rights to this article under a publishing agreement with the author(s) or other rightsholder(s); author self-archiving of the accepted manuscript version of this article is solely governed by the terms of such publishing agreement and applicable law.

© The Author(s), under exclusive licence to Springer Nature Limited 2023

Methods

Geological and preservational setting of the IVPP V31985-bearing horizon

The holotype of *F. prodigosus* (IVPP V31985) was discovered in Daxi Basin near Yangyuan Village, Zhenghe Country, Nanping City, Fujian Province, China, by the joint expedition of the Institute of Vertebrate Paleontology and Paleoanthropology (IVPP) and the Fujian Institute of Geological Survey (FIGS) from 14 October to 14 November 2022 (Fig. 4 and Extended Data Fig. 9). The IVPP V31985-bearing horizon belongs to the Nanyuan Formation, which was assigned to the Late Jurassic by a previous geological survey⁵⁹. This is confirmed by our fieldwork and radioisotopic dating (Extended Data Fig. 10). During the Late Jurassic–Early Cretaceous, southeastern China underwent intensive tectonic activity owing to the subduction of the paleo-Pacific plate, which resulted in widespread magmatism and coeval fault-depression basins^{60,61}. That geological background is essentially the same as that of the Late Jurassic period in north and northeastern China, where the older Yanliao biota is preserved^{62,63}.

To visualize the geographical distribution of the known Jurassic avialans, a palaeomap of the Late Jurassic (here, 150 Ma) was constructed using data of reconstructed coastlines and continental plates from the GPlates Web Service (<https://gwsdoc.gplates.org/>). We assembled palaeocoordinates of these Jurassic avialan-bearing horizons (the Yanliao Biota, the Solnhofen Limestones and the Nanyuan Formation in Zhenghe) from the Paleobiology Database (<https://paleobiodb.org/>; last accessed on 9 March 2023), and then plotted these sites onto the palaeomap.

The section that we excavated is 3.6 m in depth and belongs to the lower part of the Nanyuan Formation. The deposits are mainly composed of black carbonaceous mudstone and shale, interstratified with tuffite (at least four tuffite layers were recognized) (Fig. 4a). As well as IVPP V31985, we have collected numerous teleosts and more than 100 partially complete and articulated reptiles, including testudines, choristoderes and one non-avian theropod from this excavated area of around 100 m² (Fig. 4 and Extended Data Figs. 8 and 9). Considering the widely exposed contemporaneous strata that have not been investigated, the diversity and abundance of vertebrate fossils already recovered strongly indicate that this locality documents a terrestrial fauna, which we name the Zhenghe Fauna. The lithofacies and the vertebrate assemblage of the Zhenghe Fauna, which is dominated by aquatic and semi-aquatic animals, indicate that these fossiliferous sediments represent lacustrine swamp deposits. This preservational setting is different from that of the Yanliao Biota (166–159 Ma), where the fossil-bearing horizons are interpreted as freshwater lacustrine deposits^{8,62}. Some differences between these two faunas are readily appreciable, such as the absence of known teleosts, testudines and choristoderes from the Yanliao Biota^{62,64}. Future palaeontological and taphonomic studies of the Zhenghe Fauna are needed to allow more systematic comparisons with other Mesozoic biotas.

Age of the IVPP V31985-bearing horizon and the Zhenghe Fauna

Samples were collected from the tuffite layers deposited below (PM702-1) and above (PM701-4) the IVPP V31985-bearing horizon (Fig. 4a). We also collected ignimbrite samples that underlie (Bdx03) and overlie (Bdx04) the fossil-bearing sediments. Those samples were used in the zircon U-Pb dating experiments to obtain ages for the IVPP V31985-bearing horizon and the duration of the Zhenghe Fauna. Zircon samples were dated using laser ablation inductively coupled plasma mass spectrometry (LA-ICP-MS) at the Testing Center of Shandong Bureau of China Metallurgical Geology Bureau, using a Thermo Fisher Scientific X2 ICP-MS connected to a GeoLas Pro 193-nm laser ablation system. The detailed experimental procedure is outlined in ref. 65. Measurements were taken using Zircon 91500 as the external standard with a ²⁰⁷Pb/²³⁵U age of 1063.35 Ma, and a ²⁰⁶Pb/²³⁸U age of 1062.4 Ma.

Elemental contents were calculated with NIST610 as the external standard and Zr as the internal standard. The U-Pb isotope ratios and contents were calculated using the software ICPMSDataCal. Isoplot (v.3.0) was used to plot the concordia diagram and to calculate the weighted mean U-Pb age⁶⁶. The laser ablation inductively coupled plasma mass spectrometry (LA-ICP-MS) method of dating produced concordant zircon U-Pb ages of 150.2 ± 1.1 Ma (PM702-1) and 149.9 ± 1.1 Ma (PM701-4) for the lower and upper layers of the IVPP V31985-bearing horizons, respectively (Extended Data Fig. 10). Concordant zircon U-Pb ages of 150 ± 1.8 Ma (Bdx03) and 148 ± 1.9 Ma (Bdx04) were obtained from the ignimbrite samples. Together, these results constrain the Zhenghe Fauna to a time interval of 148–150 Ma.

Laser-stimulated fluorescence imaging

Laser-stimulated fluorescence images were produced using a 500-mW, 450-nm blue laser (MDL-III-450-1W, Changchun New Industries Optoelectronics Tech. Co.), with an LP-500-62 light yellow long-pass filter and a Nikon D850.

Phylogenetic analyses

To investigate the phylogenetic position of IVPP V31985, we scored this taxon into the current version of the Theropod Working Group matrix with extensive modifications^{2,67,68}. As well as IVPP V31985, we added the scansoriopterygid *Yi qi* and nine Cretaceous avialans that represent the early-diverging members of the major clades of Mesozoic avialans: the basal pygostylians *Eoconfuciusornis zhengi*, *Yangavis confucii*, *Changchengornis hengdaoziensis*, *Jinguoformis perplexus*, *Chongmingia zhengi* and *Cratonavis zhui*; the basal enantiornithine *Eopengornis martini*; and the basal ornithuromorphs *Archaeorhynchus spatula* and *Schizooura lii*. Inclusion of these early avialans could help us to understand character changes across the theropod–bird transition in broader phylogenetic scope. In addition, character scores of taxa have been revised on the basis of direct observations of the holotype specimens, new published referred materials and computed tomography data (Supplementary Information). The revised data matrix contains 853 characters and 167 taxa.

Maximum parsimony analyses were performed using the TNT software package (v.1.5)⁶⁹, with all characters equally weighted. The New Technology search method, with sectorial search, ratchet, tree drift and tree fusion, was used to conduct an heuristic tree search, with the shortest tree found in 20 replicates to recover as many tree islands as possible. The resulting most-parsimonious trees were fed into another round of branch swapping using the traditional tree-bisection-reconnection method to explore treespace more extensively. Bremer and bootstrap values were calculated as support indices. Bremer values were calculated using the Bremer script embedded in TNT, and the bootstrap values were calculated using 1,000 replicates with the same setting as in the primary search. In the strict consensus tree, IVPP V31985 was resolved in a clade (Anchiornithidae, sensu stricto⁵¹) that unites *Anchiornis*, *Aurornis*, *Xiaotingia* and *Eosinopteryx*, and the interrelationships among these taxa were unresolved (Extended Data Fig. 5). This clade Anchiornithidae emerges as the sister to the clade that contains *Archaeopteryx* and other avialans, and thus represents the earliest-branching group of the Avialae. The monophyly of the Deinonychosauria was supported in this study by recovering the sister relationship between troodontids and dromaeosaurids. Notably, the scansoriopterygids were recovered as the sister to the Oviraptorosauria, as in some previous studies^{52,70}. The phylogenetic placement of scansoriopterygids has long been debated, and has been placed in different positions; for example, as the sister to avialans or to paravians^{2,19}.

Bayesian tip-dating analysis was conducted in MrBayes v.3.2.8 (ref. 71). The Mk model⁷² with gamma rate variation across characters⁷³ was used for the morphological characters. The prior for the time tree was modelled by the fossilized birth–death process⁷⁴. The root age was assigned an offset-exponential prior with a mean age of 180 Ma and

minimum age of 170 Ma, referring to the oldest fossil. The fossil ages were given uniform distributions based on the corresponding stratigraphic ranges. The extant-sampling probability was fixed to 0.0005 based on the basis of the number of living bird species. The prior for the evolutionary rate was modelled by the uncorrelated lognormal and gamma mixed clock⁷⁵, in which the mean evolutionary rate was assigned an exponential prior with mean 0.01 (about one change per character per 100 million years) and the variance parameter was given an exponential prior with mean 1.0. We executed two independent runs and four chains per run (one cold chain and three hot chains with temperature 0.06) in Markov chain Monte Carlo. Each run was executed for 80 million generations and sampled every 2,000 generations. The first 25% samples were discarded as burn-in and the rest from the two runs were combined. Good convergence and mixing were diagnosed by an effective sample size larger than 100 for all parameters and an average standard deviation of split frequencies⁷¹ smaller than 0.01. The posterior trees were summarized as a 50% majority-rule consensus tree (Extended Data Fig. 6).

Phylogenetic comparative analyses

To compare the body shape of IVPP V31985 with other Mesozoic avialan and non-avialan theropods, we performed phylogenetic comparative analyses of the lengths of the appendicular limb segments. Length measurements of the forelimb (humerus, ulna, radius and metacarpal II) and hindlimb (femur, tibia and metatarsal III) from major groups of theropods were collected through direct measurement and published data^{13,16} (Supplementary Table 2). We only included specimens that preserved complete length for all six limb segments, given the controversy that exists with regard to scaling relationships of limb size. All of the sampled specimens were subadults or adults on the basis of the well-ossified periosteal surface of preserved bones, fusion degree of compound bones and bone histology, whenever this information was available. The dataset contained 153 species, spanning the whole spectrum of Mesozoic theropod phylogeny. The length measurements were \log_{10} -transformed to normalize the distribution before downstream analyses. An informal super tree that encompassed all taxa included in the limb dataset was assembled based on our previous studies targeting the phylogeny of Mesozoic theropods^{2,16,67,76,77}. To account for taxa with inconsistent phylogenetic positions in the literature, branches subtending to those taxa were collapsed as polytomies. The super tree was time-scaled using tip dates bounded by the first and last appearance datum of the geological stages or epochs in which a given species was discovered. This was performed using the ‘minimum branch length’ method embedded in the timePaleoPhy function in the R package paleotree⁷⁸. To account for size-dependent limb measurements^{79–81}, the \log_{10} -transformed length data were size-corrected against body mass using the `phyl.resid` function in the R package `phytools`⁸⁰. The body mass of Mesozoic theropods including *Fujianvenator* was estimated using a published empirical equation based on the diameter of the femoral shaft¹³. We performed pPCA using the size-corrected length residues to account for non-independence in trait values between species because of shared phylogeny⁸². pPCA was applied to all the limb segments, the forelimb and the hindlimb, respectively, to investigate the patterns of changes in different aspects, using the `phyl.pca` function in the R package `phytools`⁸⁰. Both two- and three-dimensional phylomorphospace was constructed to illustrate the evolutionary changes of limb proportion across the theropod tree (Fig. 3 and Extended Data Fig. 4). We also conducted conventional PCA without accounting for phylogeny and body size (Supplementary Tables 6 and 7 and Supplementary Figs. 1 and 2).

Morphometric analyses of hindlimb

To further investigate the hindlimb of *Fujianvenator* and its ecological implications, a ternary plot of the proportions of the hindlimb segments—femur, tibia and metatarsal III—was built, using the aforementioned length dataset with the addition of 535 crown birds that

span the whole avian crown phylogeny and ecologies⁸³ (Supplementary Table 3). *Fujianvenator* is spaced far away from Mesozoic theropods and is located at the periphery of the morphospace of modern waders and swimmers (Extended Data Fig. 7). Despite the similar hindlimb proportions to some modern swimming birds, we refrain from suggesting such highly specialized ecology for *Fujianvenator*, considering the absence of morphological features that are regarded to be indicators of aquatic adaptation, such as the large cnemial crests of the tibia (present in early avialans such as *Gansus* that are inferred to be aquatic or semi-aquatic)^{84,85}. The vertically oriented pubes make the pelvis dorsoventrally deep, contrasting with the streamlined body shape that is seen in aquatic birds. The gracile metatarsals are also markedly different from the mediolaterally wide and dorsoventrally flattened form seen in aquatic birds (for example, *Hesperornis* and penguins)⁸⁵. Elongated distal leg segments are widely seen in crown waders, and we posit that a wader-like ecology is possible for *Fujianvenator*, which is also consistent with the swamp-like palaeoenvironment inferred for this locality.

The elongation of the lower leg (tibia and metatarsus) is widely considered to be a reliable index of running capability among modern vertebrates^{56,57}, because of the increased stride length in each step^{58,86}. Following that, the notably elongated tibia and metatarsals preserved in *Fujianvenator* are likely to reflect its adaptation to terrestrial locomotion. To test this hypothesis, a numeric measure—cursorial limb proportion (CLP) scores⁵⁸—was calculated as a quantifiable index of cursoriality of *Fujianvenator*, non-avialan theropods and other Jurassic avialans. A detailed methodology of CLP has been described previously⁵⁸. In short, CLP scores describe the relative elongation of the lower leg by measuring the differences between the actual lower leg length and that predicted on the basis of the scaling relationship with the femur. A species with a large CLP score is interpreted to be a good ‘runner’. We extract hindlimb measurements from the dataset described above that was used in pPCA, combined with additional non-avialan theropods sampled in a previous study⁵⁸. This dataset contains 79 species (Supplementary Table 3), including specimens from all major theropod clades, particularly those that are considered good ‘runners’. The length measurements of hindlimb segments were \log_{10} -transformed before downstream analyses. We used standard major axis (SMA) regression to investigate the scaling relationship between lower leg and femur. The SMA and statistical tests were performed using the R packages `smatr` and `lmodel2`^{87,88}. Then, the CLP scores were calculated as described previously⁵⁸. Our study shows that *Fujianvenator* has the highest CLP score (43.86)—significantly larger than in *Anchiornis* (17.12), *Archaeopteryx* (4.56), troodontids, dromaeosaurids, and tyrannosauroids—suggesting that *Fujianvenator* is well adapted to terrestrial locomotion.

Reporting summary

Further information on research design is available in the Nature Portfolio Reporting Summary linked to this article.

Data availability

The specimen (IVPP V31985) described in this study is archived and available on request from the Institute of Vertebrate Paleontology and Paleoanthropology, Chinese Academy of Sciences. Phylogenetic data matrices that support the findings of this research are included as Supplementary Information. The raw data used in morphometric analyses are available at figshare (<https://doi.org/10.6084/m9.figshare.22548385>). The Life Science Identifier for *Fujianvenator* is urn:lsid:zoobank.org:act:E47B6E41-4D48-40A1-B3CD-974D84A1E53E.

Code availability

The R code used in morphometric analyses is available at figshare (<https://doi.org/10.6084/m9.figshare.22548385>).

minimum age of 170 Ma, referring to the oldest fossil. The fossil ages were given uniform distributions based on the corresponding stratigraphic ranges. The extant-sampling probability was fixed to 0.0005 based on the basis of the number of living bird species. The prior for the evolutionary rate was modelled by the uncorrelated lognormal and gamma mixed clock⁷⁵, in which the mean evolutionary rate was assigned an exponential prior with mean 0.01 (about one change per character per 100 million years) and the variance parameter was given an exponential prior with mean 1.0. We executed two independent runs and four chains per run (one cold chain and three hot chains with temperature 0.06) in Markov chain Monte Carlo. Each run was executed for 80 million generations and sampled every 2,000 generations. The first 25% samples were discarded as burn-in and the rest from the two runs were combined. Good convergence and mixing were diagnosed by an effective sample size larger than 100 for all parameters and an average standard deviation of split frequencies⁷¹ smaller than 0.01. The posterior trees were summarized as a 50% majority-rule consensus tree (Extended Data Fig. 6).

Phylogenetic comparative analyses

To compare the body shape of IVPP V31985 with other Mesozoic avialan and non-avialan theropods, we performed phylogenetic comparative analyses of the lengths of the appendicular limb segments. Length measurements of the forelimb (humerus, ulna, radius and metacarpal II) and hindlimb (femur, tibia and metatarsal III) from major groups of theropods were collected through direct measurement and published data^{13,16} (Supplementary Table 2). We only included specimens that preserved complete length for all six limb segments, given the controversy that exists with regard to scaling relationships of limb size. All of the sampled specimens were subadults or adults on the basis of the well-ossified periosteal surface of preserved bones, fusion degree of compound bones and bone histology, whenever this information was available. The dataset contained 153 species, spanning the whole spectrum of Mesozoic theropod phylogeny. The length measurements were \log_{10} -transformed to normalize the distribution before downstream analyses. An informal super tree that encompassed all taxa included in the limb dataset was assembled based on our previous studies targeting the phylogeny of Mesozoic theropods^{2,16,67,76,77}. To account for taxa with inconsistent phylogenetic positions in the literature, branches subtending to those taxa were collapsed as polytomies. The super tree was time-scaled using tip dates bounded by the first and last appearance datum of the geological stages or epochs in which a given species was discovered. This was performed using the ‘minimum branch length’ method embedded in the timePaleoPhy function in the R package paleotree⁷⁸. To account for size-dependent limb measurements^{79–81}, the \log_{10} -transformed length data were size-corrected against body mass using the `phyl.resid` function in the R package `phytools`⁸⁰. The body mass of Mesozoic theropods including *Fujianvenator* was estimated using a published empirical equation based on the diameter of the femoral shaft¹³. We performed pPCA using the size-corrected length residues to account for non-independence in trait values between species because of shared phylogeny⁸². pPCA was applied to all the limb segments, the forelimb and the hindlimb, respectively, to investigate the patterns of changes in different aspects, using the `phyl.pca` function in the R package `phytools`⁸⁰. Both two- and three-dimensional phylomorphospace was constructed to illustrate the evolutionary changes of limb proportion across the theropod tree (Fig. 3 and Extended Data Fig. 4). We also conducted conventional PCA without accounting for phylogeny and body size (Supplementary Tables 6 and 7 and Supplementary Figs. 1 and 2).

Morphometric analyses of hindlimb

To further investigate the hindlimb of *Fujianvenator* and its ecological implications, a ternary plot of the proportions of the hindlimb segments—femur, tibia and metatarsal III—was built, using the aforementioned length dataset with the addition of 535 crown birds that

span the whole avian crown phylogeny and ecologies⁸³ (Supplementary Table 3). *Fujianvenator* is spaced far away from Mesozoic theropods and is located at the periphery of the morphospace of modern waders and swimmers (Extended Data Fig. 7). Despite the similar hindlimb proportions to some modern swimming birds, we refrain from suggesting such highly specialized ecology for *Fujianvenator*, considering the absence of morphological features that are regarded to be indicators of aquatic adaptation, such as the large cnemial crests of the tibia (present in early avialans such as *Gansus* that are inferred to be aquatic or semi-aquatic)^{84,85}. The vertically oriented pubes make the pelvis dorsoventrally deep, contrasting with the streamlined body shape that is seen in aquatic birds. The gracile metatarsals are also markedly different from the mediolaterally wide and dorsoventrally flattened form seen in aquatic birds (for example, *Hesperornis* and penguins)⁸⁵. Elongated distal leg segments are widely seen in crown waders, and we posit that a wader-like ecology is possible for *Fujianvenator*, which is also consistent with the swamp-like palaeoenvironment inferred for this locality.

The elongation of the lower leg (tibia and metatarsus) is widely considered to be a reliable index of running capability among modern vertebrates^{56,57}, because of the increased stride length in each step^{58,86}. Following that, the notably elongated tibia and metatarsals preserved in *Fujianvenator* are likely to reflect its adaptation to terrestrial locomotion. To test this hypothesis, a numeric measure—cursorial limb proportion (CLP) scores⁵⁸—was calculated as a quantifiable index of cursoriality of *Fujianvenator*, non-avialan theropods and other Jurassic avialans. A detailed methodology of CLP has been described previously⁵⁸. In short, CLP scores describe the relative elongation of the lower leg by measuring the differences between the actual lower leg length and that predicted on the basis of the scaling relationship with the femur. A species with a large CLP score is interpreted to be a good ‘runner’. We extract hindlimb measurements from the dataset described above that was used in pPCA, combined with additional non-avialan theropods sampled in a previous study⁵⁸. This dataset contains 79 species (Supplementary Table 3), including specimens from all major theropod clades, particularly those that are considered good ‘runners’. The length measurements of hindlimb segments were \log_{10} -transformed before downstream analyses. We used standard major axis (SMA) regression to investigate the scaling relationship between lower leg and femur. The SMA and statistical tests were performed using the R packages `smatr` and `lmodel2`^{87,88}. Then, the CLP scores were calculated as described previously⁵⁸. Our study shows that *Fujianvenator* has the highest CLP score (43.86)—significantly larger than in *Anchiornis* (17.12), *Archaeopteryx* (4.56), troodontids, dromaeosaurids, and tyrannosauroids—suggesting that *Fujianvenator* is well adapted to terrestrial locomotion.

Reporting summary

Further information on research design is available in the Nature Portfolio Reporting Summary linked to this article.

Data availability

The specimen (IVPP V31985) described in this study is archived and available on request from the Institute of Vertebrate Paleontology and Paleoanthropology, Chinese Academy of Sciences. Phylogenetic data matrices that support the findings of this research are included as Supplementary Information. The raw data used in morphometric analyses are available at figshare (<https://doi.org/10.6084/m9.figshare.22548385>). The Life Science Identifier for *Fujianvenator* is urn:lsid:zoobank.org:act:E47B6E41-4D48-40A1-B3CD-974D84A1E53E.

Code availability

The R code used in morphometric analyses is available at figshare (<https://doi.org/10.6084/m9.figshare.22548385>).

60. Wang, D. & Shu, L. Late Mesozoic basin and range tectonics and related magmatism in Southeast China. *Geosci. Front.* **3**, 109–124 (2012).
61. Zhao, J., Qiu, J. & Liu, L. Early–Middle Jurassic magmatic rocks along the coastal region of southeastern China: petrogenesis and implications for paleo-Pacific plate subduction. *J. Asian Earth Sci.* **210**, 104687 (2021).
62. Zhou, Z. & Wang, Y. Vertebrate assemblages of the Jurassic Yanliao Biota and the Early Cretaceous Jehol Biota: comparisons and implications. *Palaeoworld* **26**, 241–252 (2017).
63. Zhu, R., Zhou, Z. & Meng, Q. Destruction of the North China Craton and its influence on surface geology and terrestrial biotas. *Chin. Sci. Bull.* **65**, 2954 (2020).
64. Sullivan, C. et al. The vertebrates of the Jurassic Daohugou Biota of northeastern China. *J. Vertebr. Paleontol.* **34**, 243–280 (2014).
65. Liu, Y. et al. Continental and oceanic crust recycling-induced melt–peridotite interactions in the Trans-North China Orogen: U–Pb dating, Hf isotopes and trace elements in zircons from mantle xenoliths. *J. Petrol.* **51**, 537–571 (2009).
66. Ludwig, K. R. User’s manual for Isoplot 3.00: a geochronological toolkit for Microsoft Excel. *Berkeley Geochron. Cent. Spec. Publ.* **4**, 25–32 (2003).
67. Turner, A. H., Montanari, S. & Norell, M. A. A new dromaeosaurid from the Late Cretaceous Khulsan locality of Mongolia. *Am. Mus. Novit.* **3965**, 1–48 (2021).
68. Brusatte, S. L., Lloyd, G. T., Wang, S. C. & Norell, M. A. Gradual assembly of avian body plan culminated in rapid rates of evolution across the dinosaur–bird transition. *Curr. Biol.* **24**, 2386–2392 (2014).
69. Goloboff, P. A. & Catalano, S. A. TNT version 1.5, including a full implementation of phylogenetic morphometrics. *Cladistics* **32**, 221–238 (2016).
70. Agnolin, F. L. & Novas, F. E. *Avian Ancestors: A Review of the Phylogenetic Relationships of the Theropods Unenlagiidae, Microraptorina, Anchiornis and Scansoriopterygidae* (Springer, 2013).
71. Ronquist, F. et al. MrBayes 3.2: efficient Bayesian phylogenetic inference and model choice across a large model space. *Syst. Biol.* **61**, 539–542 (2012).
72. Lewis, P. O. A likelihood approach to estimating phylogeny from discrete morphological character data. *Syst. Biol.* **50**, 913–925 (2001).
73. Yang, Z. Maximum likelihood phylogenetic estimation from DNA sequences with variable rates over sites: approximate methods. *J. Mol. Evol.* **39**, 306–314 (1994).
74. Zhang, C., Stadler, T., Klopstein, S., Heath, T. A. & Ronquist, F. Total-evidence dating under the fossilized birth–death process. *Syst. Biol.* **65**, 228–249 (2015).
75. Zhang, C. Selecting and averaging relaxed clock models in Bayesian tip dating of Mesozoic birds. *Paleobiology* **48**, 340–352 (2022).
76. Xu, X. et al. Two Early Cretaceous fossils document transitional stages in alvarezsaurian dinosaur evolution. *Curr. Biol.* **28**, 1–8 (2018).
77. Rauhut, O. W. M. & Pol, D. Probable basal allosauroid from the early Middle Jurassic Cañadón Asfalto Formation of Argentina highlights phylogenetic uncertainty in tetanuran theropod dinosaurs. *Sci. Rep.* **9**, 18826 (2019).
78. Bapst, D. W. paleotree: an R package for paleontological and phylogenetic analyses of evolution. *Methods Ecol. Evol.* **3**, 803–807 (2012).
79. Revell, L. J. Size-correction and principal components for interspecific comparative studies. *Evolution* **63**, 3258–3268 (2009).
80. Revell, L. J. phytools: an R package for phylogenetic comparative biology (and other things). *Methods Ecol. Evol.* **3**, 217–223 (2012).
81. Grafen, A. The phylogenetic regression. *Philos. Trans. R. Soc. B* **326**, 119–157 (1989).
82. Felsenstein, J. Phylogenies and the comparative method. *Am. Nat.* **125**, 1–15 (1985).
83. Stoessel, A., Kilbourne, B. M. & Fischer, M. S. Morphological integration versus ecological plasticity in the avian pelvic limb skeleton. *J. Morphol.* **274**, 483–495 (2013).
84. You, H. et al. A nearly modern amphibious bird from the Early Cretaceous of northwestern China. *Science* **312**, 1640–1643 (2006).
85. Zinoviev, A. V. Notes on the hindlimb myology and syndesmology of the Mesozoic toothed bird *Hesperornis regalis* (Aves: Hesperornithiformes). *J. Syst. Palaeontol.* **9**, 65–84 (2011).
86. Heglund, N. C. & Cavagna, G. A. Efficiency of vertebrate locomotory muscles. *J. Exp. Biol.* **115**, 283–292 (1985).
87. Warton, D. I., Duursma, R. A., Falster, D. S. & Taskinen, S. SMATR 3—an R package for estimation and inference about allometric lines. *Methods Ecol. Evol.* **3**, 257–259 (2012).
88. Pinheiro, J. et al. nlme: Linear and nonlinear mixed-effects models. R package version 3.1-158 <https://CRAN.R-project.org/package=nlme> (2022).

Acknowledgements We thank W.-Q. Feng, Y. Li, S. Miao, J.-T. Feng and X. Lin for helping with fieldwork; Y. Li for specimen preparation; W. Gao for photography; and S. Miao and J.-T. Feng for laser-stimulated fluorescence imaging. This research was supported by the National Natural Science Foundation of China (42225201 and 42288201); the Key Research Program of Frontier Sciences, CAS (ZDBS-LY-DQC002); the New Cornerstone Science Foundation through the XPLORE PRIZE; Fujian Provincial Department of Natural Resources under the program ‘Investigation of the Geological Relics and Fossil Resources of the Late Mesozoic Basins in Western Fujian’ (GY20220108); and Fujian Provincial Bureau of Geology and Mineral Exploration and Development under the program ‘Study on the Sedimentary Environment of Dinosaur Fossils in Fujian Province’ (MDDR2021-32).

Author contributions M.W. designed the project. M.W. and L.X. supervised the fieldwork. M.W. performed the phylogenetic and comparative analyses. L.X., R.C., M.L., J.T., G.Z., L.W., W.H. and Y. L. collected samples and supervised the radioisotopic dating experiments. M.W. and C.Z. performed the tip-dating analyses. L.D., H.Y., and X.X. studied the vertebrate assemblage and paleoenvironment. M.W. and Z.Z. wrote the manuscript with input from all of the authors.

Competing interests The authors declare no competing interests.

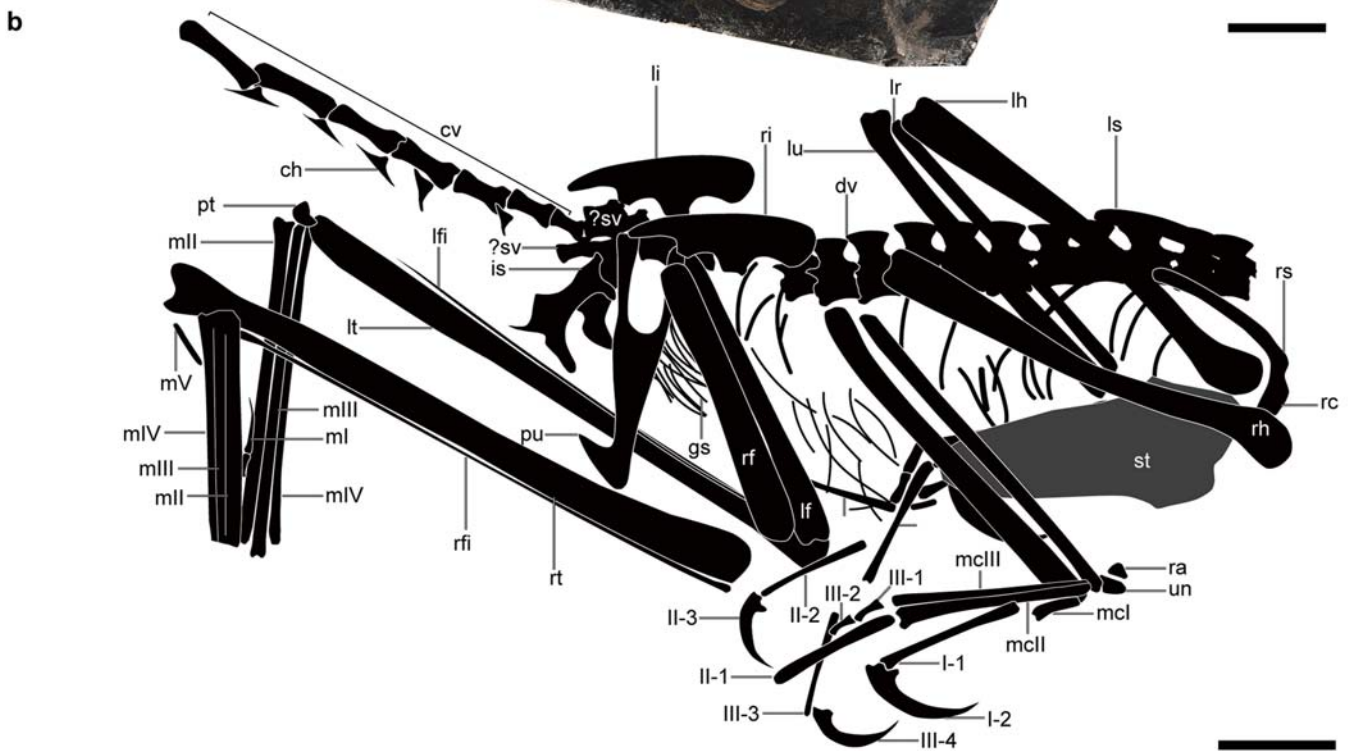
Additional information

Supplementary information The online version contains supplementary material available at <https://doi.org/10.1038/s41586-023-06513-7>.

Correspondence and requests for materials should be addressed to Min Wang.

Peer review information Nature thanks Steve Brusatte, Daniel Field and Fernando Novas for their contribution to the peer review of this work.

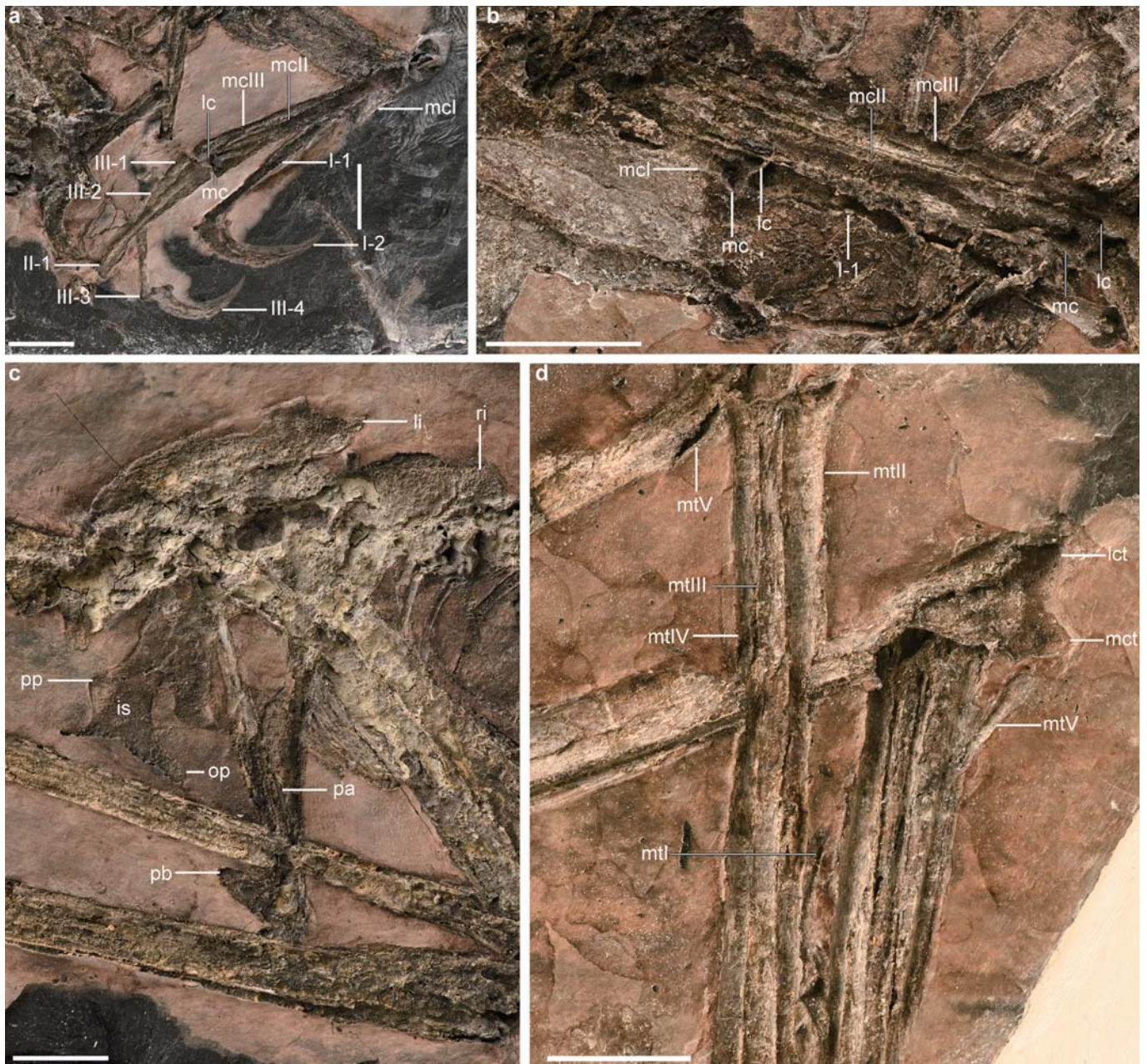
Reprints and permissions information is available at <http://www.nature.com/reprints>.



Extended Data Fig. 1 | Counter slab of holotype of *F. prodigiosus*, IVPP

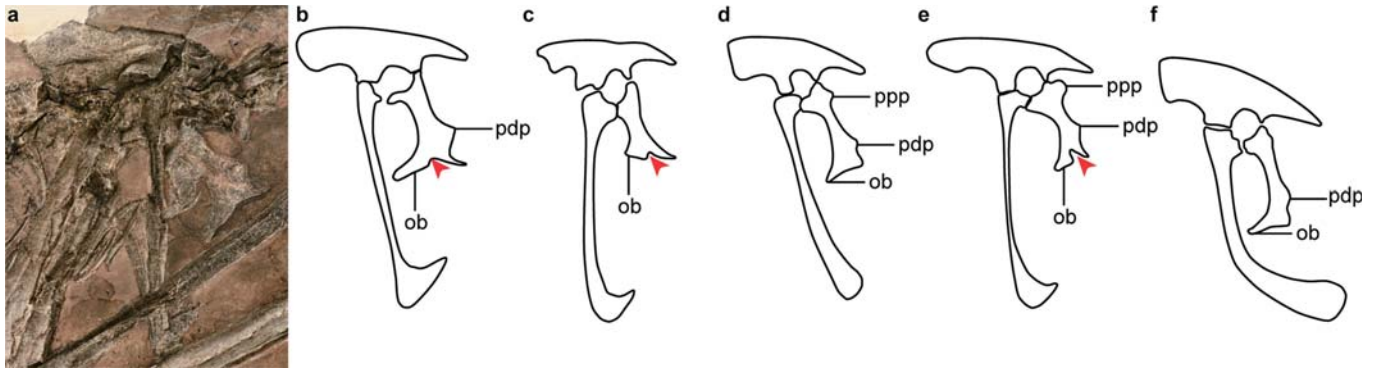
V31985. a, Photograph. **b**, Line drawing. ch, chevron; cv, caudal vertebra; dv, dorsal vertebra; gs, gastralia; lf, left femur; lfi, left fibula; lh, left humerus; li, left ilium; is, ischium; lr, left radius; ls, left scapula; lt, left tibia; lu, left ulna; ml to mV, metatarsal I to V; mcl to mIII, metacarpal I to III; pt, proximal tarsal;

pu, pubis; rh, right humerus; ra, radiale; rc, right coracoid; rf, right femur; rfi, right fibula; ri, right ilium; rs, right scapula; rt, right tibia; st, sternum; un, ulnare; ?sv, possible sacral vertebra; I-1 to I-2, manual phalanx I-1 and I-2; II-1 to II-3, manual phalanx II-1 to II-3; III-1 to III-4, manual phalanx III-1 to III-4. Scale bars, 20 mm.



Extended Data Fig. 2 | Additional anatomy of *F. prodigiosus*, IVPP V31985.
a, Right hand. **b**, Close-up of the left metacarpals. **c**, Pelvis. **d**, Proximal ends of metatarsals. is, ischium; lc, lateral condyle; lct, lateral condyle of tibiotarsus; li, left ilium; mc, medial condyle; mct, medial condyle of tibiotarsus; mcl to III,

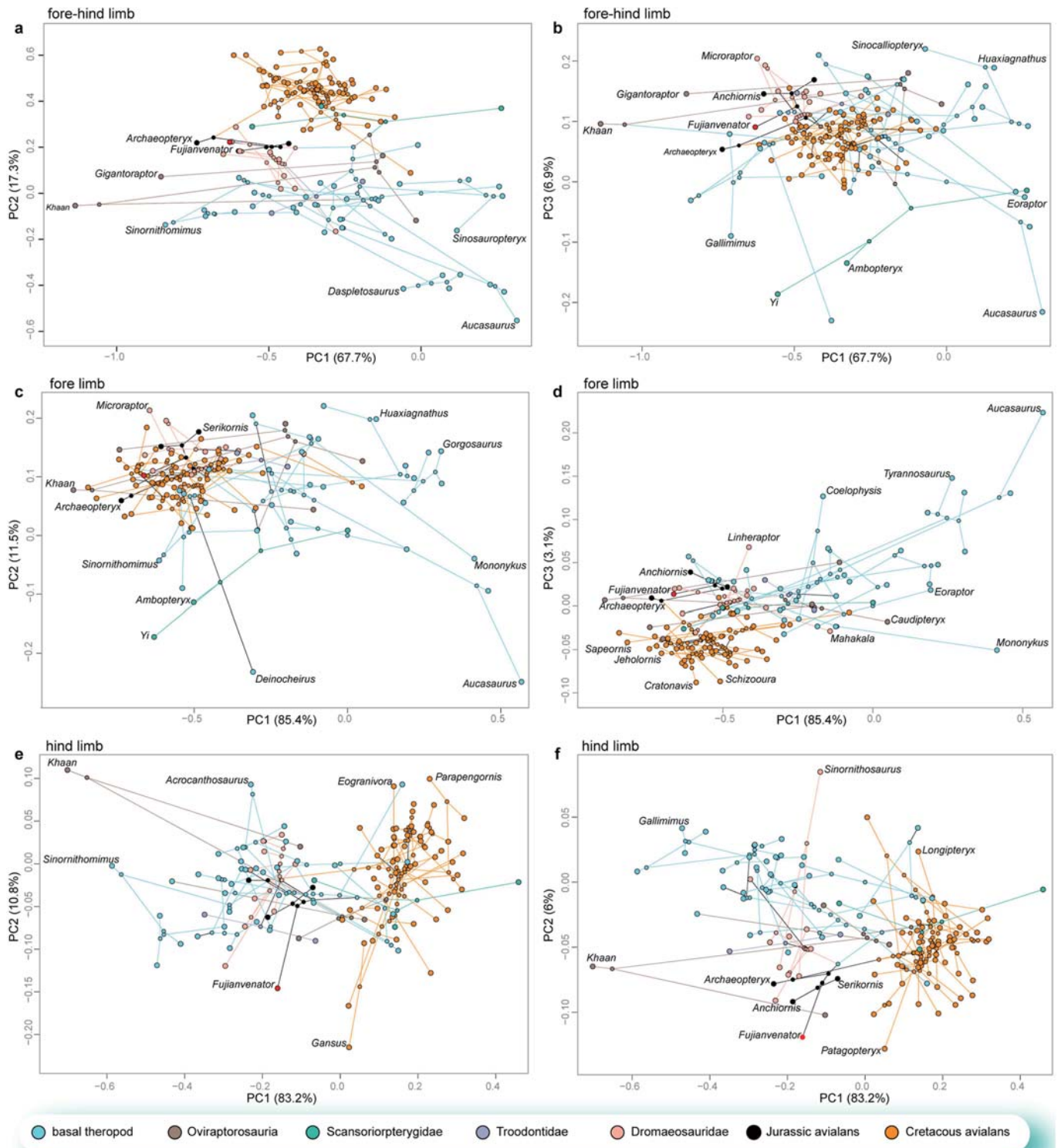
metacarpal I to III; mtl to mtV, metatarsal I to V; ob, obturator process; pa, pubic apron; pb, pubic boot; pp, posterior distal process; ri, right ilium; I-1 to I-2, manual phalanx I-1 and I-2; II-1, manual phalanx II-1; III-1 to III-4, manual phalanx III-1 to III-4. Scale bars, 10 mm.



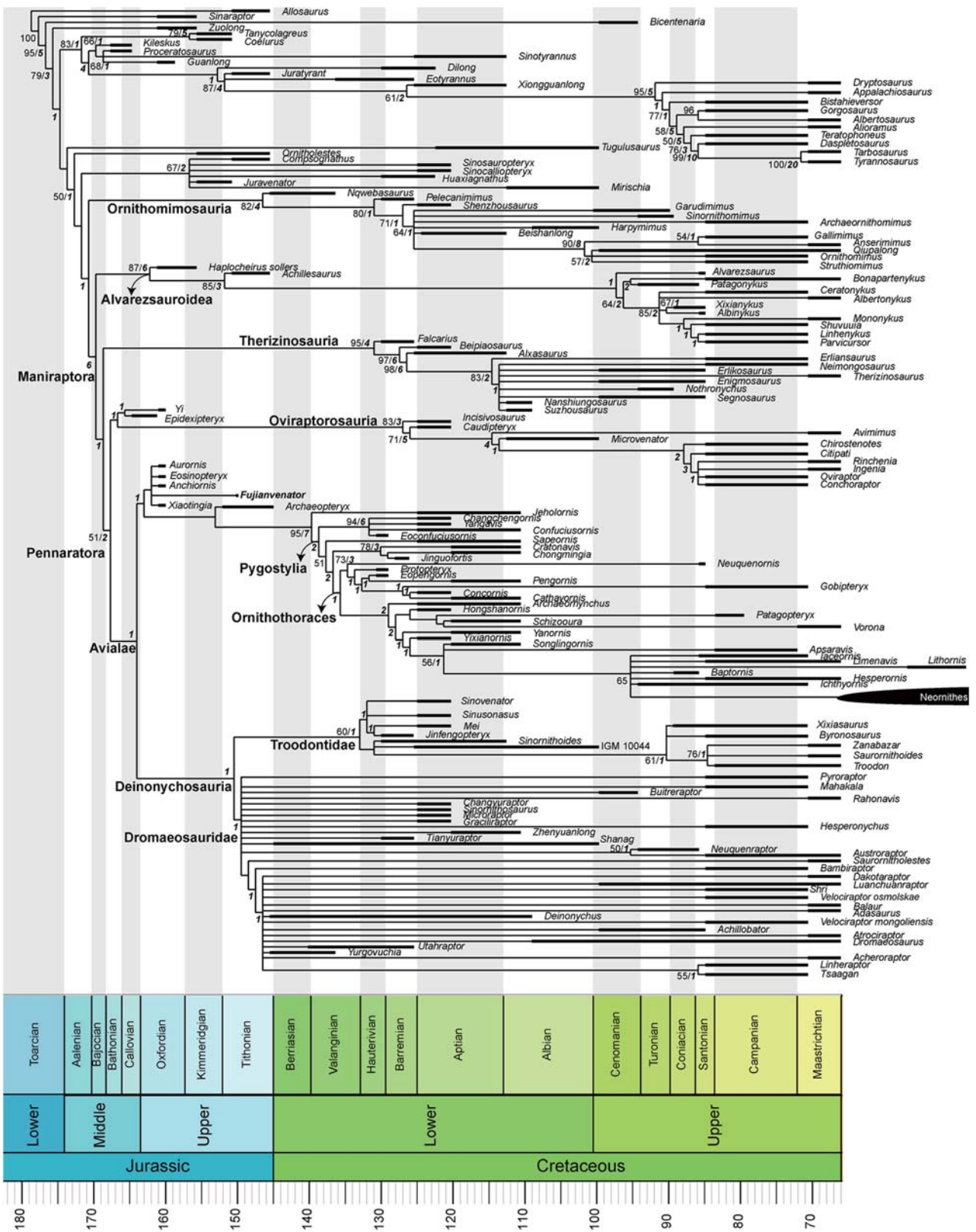
Extended Data Fig. 3 | Comparison of the pelvic anatomy of *F. prodigiosus* with that of other selected paravians. a, b. Photograph (a) and reconstruction (b) of the pelvis of *F. prodigiosus*. **c–f,** Reconstructed pelvis: avialan *Anchiornis* (c; modified from refs. 7 and 87), troodontid *Sinovenator changii* (d; modified from ref. 4), avialan *Archaeopteryx* (e; modified from ref. 4) and dromaeosaurid

Microraptor (f; modified from ref. 4). ob, obturator process; pdp, posterior distal process; ppp, posterior proximal process. The arrowheads denote the constriction at the base of the obturator process. Line drawings are not to scale.

Article

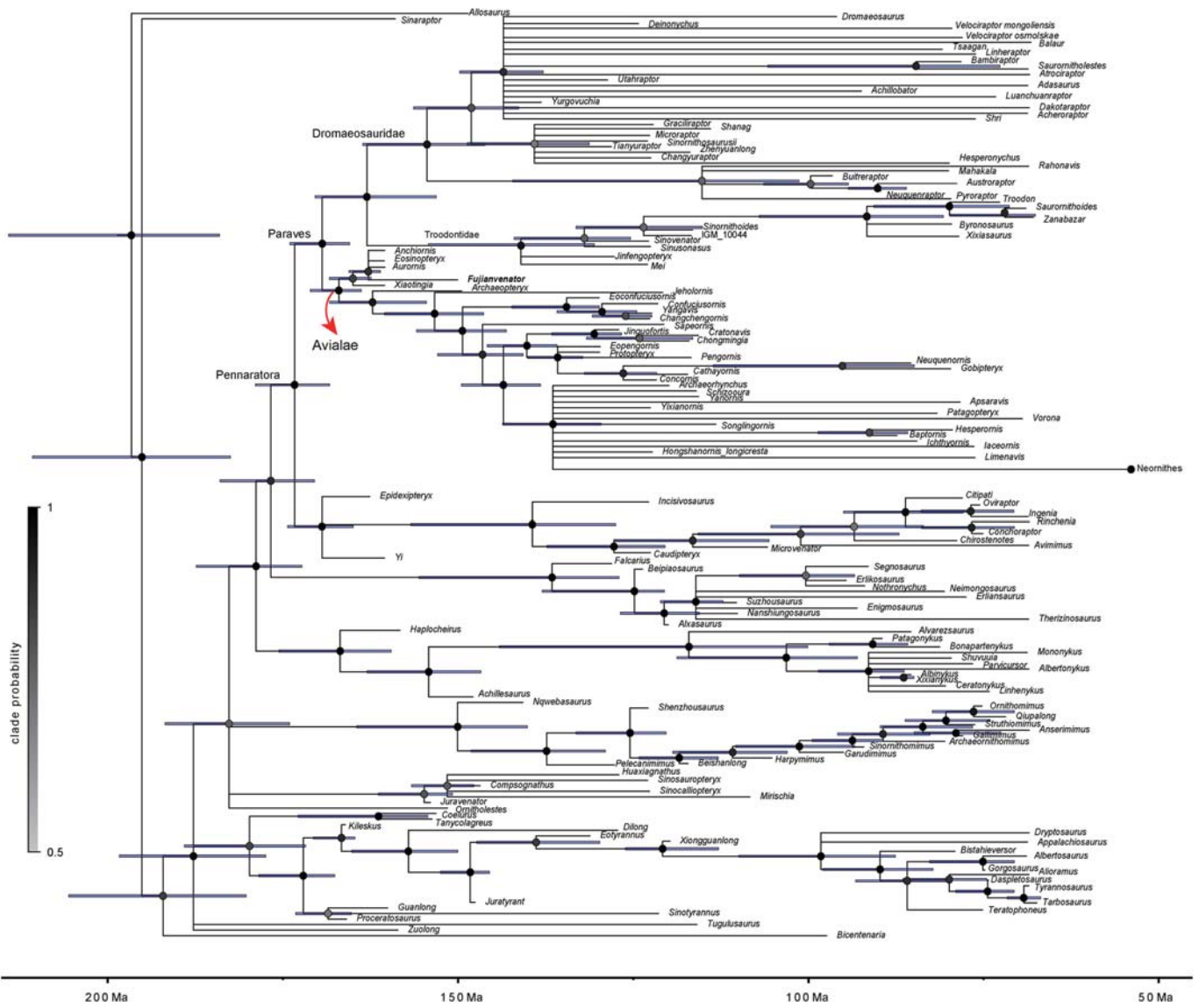


Extended Data Fig. 4 | Morphometric analyses of limb-bone length across the Mesozoic theropod phylogeny. a–f, Binary plots of the first three principal components (PCs) of the phylogenetic principal components analyses of the six limb segments (a,b), forelimb (c,d), and hindlimb (e,f).



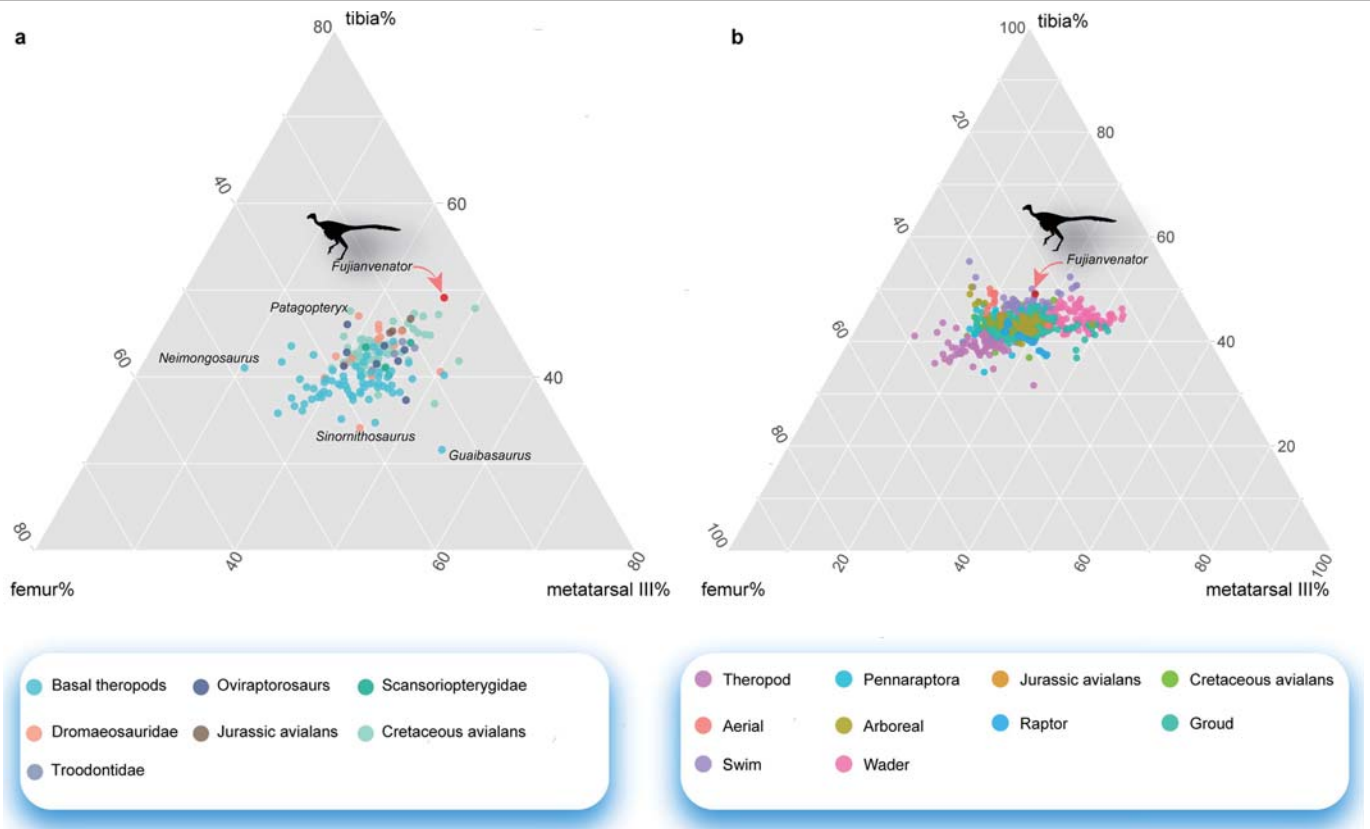
Extended Data Fig. 5 | Time-scaled phylogeny showing the position of *F. prodigiosus* through parsimony analyses. The phylogeny is the strict consensus resulting from maximum parsimony analyses. The bootstrap and

Bremer values are denoted in normal and bold italic fonts, respectively. Thick lines represent the first and last appearance datum of the geological stages or epochs in which a given species was discovered.



Extended Data Fig. 6 | Dated phylogeny showing the position of *F. prodigiosus* through Bayesian tip-dating analysis. The phylogeny is the majority-rule consensus obtained from the posterior trees of Bayesian

tip-dating analysis using the fossilized birth–death model. The error bars at the nodes represent the 95% highest posterior density intervals. The shaded circles at the nodes represent the posterior probability of the corresponding clade.



Extended Data Fig. 7 | Comparison of the hindlimb proportions of *F. prodigiosus* with those of stem and crown groups of theropods. a, b, Ternary plot of the length proportion of the hindlimb segments (femur, tibia and metatarsal III) of Mesozoic theropods (a), and with the inclusion of crown birds (b).



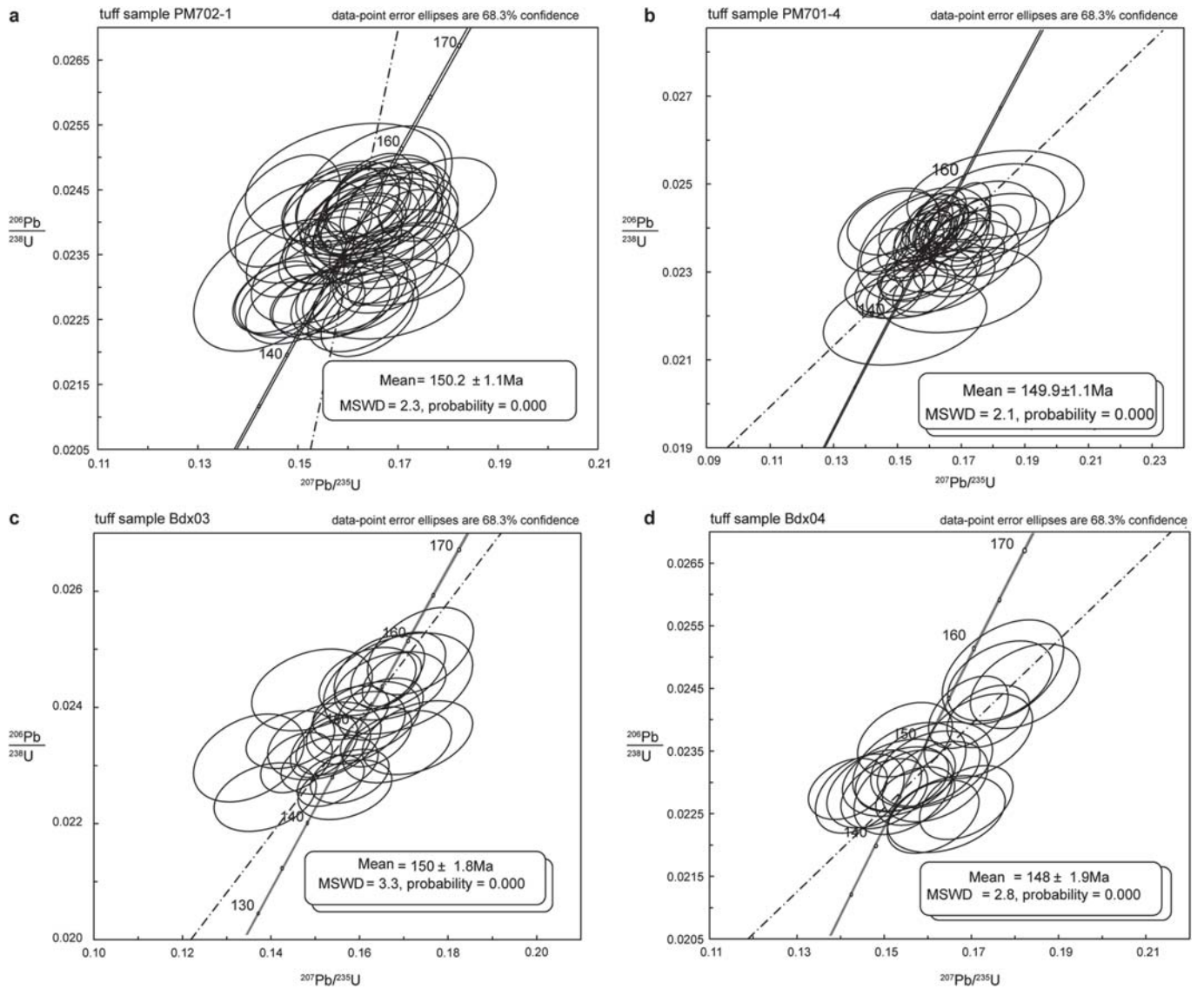
Extended Data Fig. 8 | Additional vertebrate fossils discovered in the Zhenghe Fauna during the 2022 fieldwork. a,b, Teleostei indet. (Actinopterygii: Neopterygii). **c–h**, Testudines indet. (Reptilia: Pantestudines).

i–k, Allochoristodera indet. (Reptilia: Choristodera). All photographs were taken in the field shortly after the discovery of the corresponding specimens.



Extended Data Fig. 9 | Photograph of the 2022 fieldwork in Zhenghe. Aerial shot showing the excavation area.

Article



Extended Data Fig. 10 | LA-ICP-MS concordial age plots of the fossil-bearing horizons of the Zhenghe Fauna. a, b. Samples from the tuffite layers deposited just below (c, PM702-1) and above (d, PM701-4) the IVPP V31985-bearing horizon.

c, d. Samples from the ignimbrites that underlie (a, Bdx03) and overlie (b, Bdx04) the fossil-bearing sediments.